PLOS PATHOGENS

Essential roles for deubiquitination in *Leishmania* life cycle progression

Andreas Damianou[1,2], **Rebecca J. Burge**[1], **Carolina M. C. Catta-Preta**[1], **Vincent Geoghegan**[1], **Y. Romina Nievas**[1], **Katherine Newling**[1], **Elaine Brown**[1], **Richard Burchmore**[2], **Boris Rodenko**[3], **Jeremy C. Mottram**[1] *

1 York Biomedical Research Institute and Department of Biology, University of York, United Kingdom, **2** Wellcome Centre for Integrative Parasitology, Institute of Infection, Immunity and Inflammation, College of Medical Veterinary and Life Sciences, University of Glasgow, Glasgow, United Kingdom, **3** UbiQ Bio BV, Amsterdam Science Park, The Netherlands

* jeremy.mottram@york.ac.uk

Abstract

The parasitic protozoan *Leishmania* requires proteasomal, autophagic and lysosomal proteolytic pathways to enact the extensive cellular remodelling that occurs during its life cycle. The proteasome is essential for parasite proliferation, yet little is known about the requirement for ubiquitination/deubiquitination processes in growth and differentiation. Activity-based protein profiling of *L. mexicana* C12, C19 and C65 deubiquitinating cysteine peptidases (DUBs) revealed DUB activity remains relatively constant during differentiation of procyclic promastigote to amastigote. However, when life cycle phenotyping (bar-seq) was performed on a pool including 15 barcoded DUB null mutants created in promastigotes using CRISPR-Cas9, significant loss of fitness was observed during differentiation and intracellular infection. DUBs 4, 7, and 13 are required for successful transformation from metacyclic promastigote to amastigote and DUBs 3, 5, 6, 8, 10, 11 and 14 are required for normal amastigote proliferation in mice. DUBs 1, 2, 12 and 16 are essential for promastigote viability and the essential role of DUB2 in establishing infection was demonstrated using DiCre inducible gene deletion *in vitro* and *in vivo*. DUB2 is found in the nucleus and interacts with nuclear proteins associated with transcription/chromatin dynamics, mRNA splicing and mRNA capping. DUB2 has broad linkage specificity, cleaving all the di-ubiquitin chains except for Lys27 and Met1. Our study demonstrates the crucial role that DUBs play in differentiation and intracellular survival of *Leishmania* and that amastigotes are exquisitely sensitive to disruption of ubiquitination homeostasis.

Author summary

Leishmania parasites require a variety of protein degradation pathways to enable the parasite to transition through the various life cycle stages that occur in its insect and mammalian hosts. Several enzymes involved in protein degradation in *Leishmania* are known to be essential, including a multi-protein complex, the proteasome, but little is known about how proteins are targeted to the proteasome for degradation. Here, we analyse

---

---

components of the deubiquitination pathway, including twenty cysteine peptidases (DUBs) that remove the posttranslational modifier ubiquitin from substrates tagged for proteasomal degradation. We used chemical probes to measure active enzymes in parasite lysates and genome engineering to create DUB gene deletion mutants. We identified some DUBs that are essential for parasite viability and some that are required for life cycle progression. We carried out a detailed analysis of the essential DUB2, which has broad deubiquitinase activity and is found in the nucleus. This enzyme interacts with nuclear proteins associated with transcription/chromatin dynamics, mRNA splicing and mRNA capping. This work demonstrates the important role that DUBs play in *Leishmania in vivo* infection and further validates DUBs as potential drug targets in this parasite.

Introduction

Leishmaniasis is a vector-borne neglected tropical disease that causes serious public health problems in 98 tropical and sub-tropical countries and is responsible for 20,000–40,000 deaths annually [1]. The disease spectrum varies from asymptomatic infection, through a disfiguring and debilitating mucocutaneous form to a visceral form that can be fatal. The causative agent of this disease is the obligate intracellular parasite of the genus *Leishmania*. The developmental process of *Leishmania* is closely linked with the ability of this parasite to survive and replicate in distinct environmental niches. The medical importance of one of these environmental niches is evident in the phagolysosomes of the infected host macrophages, where the *Leishmania* parasites differentiate from the motile promastigote to the non-motile amastigote and subsequently proliferate and establish an infection. The morphological and transcriptional changes that occur after differentiation of *Leishmania* promastigotes to amastigotes are well established [2], but little is known about the regulatory and operational processes that underpin this transition. Reversible post-translational modification (PTM) of proteins with chemical groups, such as phosphorylation, or other proteins, such as ubiquitination, are likely to be pivotal for successful life cycle progression [3–5] and intracellular parasitism. In addition, irreversible PTM such as proteolytic cleavage is important for the cellular remodeling that occurs during the life cycle of *Leishmania* and the commitment to differentiation[6–8], as well as in amastigote survival [9, 10].

Ubiquitination is an evolutionarily conserved post-translational modification involving a series of highly regulated enzymatic reactions resulting in attachment of ubiquitin to proteins in the cell [11]. Ubiquitination regulates vital cellular mechanisms including protein degradation through the ubiquitin-proteasome system (UPS), autophagy, DNA repair and protein trafficking. For the covalent attachment of ubiquitin to target protein or other ubiquitin, three types of enzymes are required to act sequentially: E1 ubiquitin-activating enzyme, E2 ubiquitin-conjugating enzyme and an E3 ubiquitin ligase [11]. This system is reversible and deubiquitinase enzymes (DUBs) are responsible for the removal of ubiquitin from the target protein, providing an additional level of regulation of the ubiquitination pathway [12]. The number of DUBs varies from organism to organism. For example, around 100 DUBs have been discovered in humans but only 20 DUBs have been found in *Saccharomyces cerevisiae* [13]. In general, DUBs can be divided into seven distinct structural families [14]: ubiquitin-specific proteases (USPs, family C19), C-terminal hydrolyses (UCHs, family C12), ovarian tumor proteases (OTUs, family C65), JAB1/MPN/MOV34 metalloenzymes (JAMM/MPN+, family M67), Josephins, family C86, MINDY, family C115 [15] and the newly identified ZUFSP (zinc finger with UFM1-specific peptidase domain protein), family C78 [13, 15]. Here

we characterise DUBs of *Leishmania* and describe a bar-seq CRISPR-Cas9 genome editing strategy that was used to evaluate the requirement for DUB activity in the *Leishmania* life cycle. Our data demonstrate that the broad and diverse mechanisms used by DUBs are required for successful *Leishmania* life cycle progression.

Results

Leishmania deubiquitinase cysteine peptidase gene family

We searched the genome of *L. mexicana* and identified 20 DUBs belonging to the C12, C19 and C65 families (S1 Table). Nineteen of these 20 DUBs are conserved in the closely related trypanosomatid *Trypanosoma brucei*, with only the C19 family DUB18 being absent. Domain analysis using InterPro [16] confirmed the presence of the expected DUB peptidase domains. Furthermore, several other domains including UBA [17], zinc finger UBP-type [18], WD40, exonuclease RNase and PAN2 domains were also identified (Fig 1A).

A phylogenetic tree of *L. mexicana* and *Homo sapiens* DUBs revealed the clustering of *Leishmania* DUBs into human DUB families. DUB15 and DUB16 clustered with mammalian C12 UCH DUBs and DUB17 with mammalian C65 OTU as expected (Fig 1B). USP (C19) DUBs are the largest class of DUBs in humans (~60 members) and also in *L. mexicana* (17 members). Most of the USPs include domains in addition to their C19 catalytic domain. The C19 DUBs have limited sequence conservation, restricted to the catalytic domain which consists of an active catalytic triad including Cys, His and Asp or Asn residues. The rest of the protein sequence is highly diverse among the USPs and it is believed that this sequence diversity is crucial for the substrate recognition through interaction with other proteins.

Sequence alignments revealed that all of the DUBs contained the catalytic triad except for DUB13, which has an Asn in place of the consensus His (S1 Fig). DUB13 is the orthologue of human USP52, also known as PAN2, a subunit of the deadenylation complex [19]. PAN2 lacks some of the catalytic triad residues in the DUB domain that are thought to be important for DUB activity including the active Cys [20], yet PAN2 is able to cleave K6-, K11-, K48-, K63-, and M1-linked ubiquitin chains, suggesting that specific post-translational modifications or protein folding could rearrange its active site to form a new active centre [21].

Leishmania DUBs required for life cycle transition

The fluorescent activity-based probe (ABP) Cy5UbPRG, previously developed for its ability to react with active DUBs [22], identified active DUBs in the lysate of *L. mexicana* promastigotes. In-gel fluorescence (Cy5) showed the presence of several DUBs in the range of 30–160 kDa (Fig 2A), the size expected taking into account the covalent attachment of the 9 kDa Cy5UbPRG probe (S1 Table). The activity of DUBs detected with the ABP was similar in promastigotes, axenic amastigotes and lesion-derived amastigotes and during differentiation from amastigotes to promastigotes (Fig 2B). UbPRG was then attached to Sepharose beads and used to affinity purify proteins from an *L. mexicana* promastigote cell lysate, and mass spectrometry used to confirm DUB identity. Six DUBs (DUB2, DUB15, DUB16, DUB17, DUB18, and DUB19) were successfully identified only in the UbPRG sample and not in the control sample, indicating that the warhead can successfully react with cysteine peptidase DUBs (Fig 2C and S2A Table). Twenty other proteins specifically identified in the UbPRG sample are likely to be proteins that are DUB substrates (such as polyubiquitin, LmxM.09.0891), form complexes with DUBs, or react directly with the PRG warhead.

To assess whether the 20 DUBs were dispensable for growth of *L. mexicana* promastigotes each gene was targeted for deletion using CRISPR-Cas9 [23] with two barcoded antibiotic resistance cassettes to attempt to replace both allelic copies of each *DUB* (Fig 2C). In the first
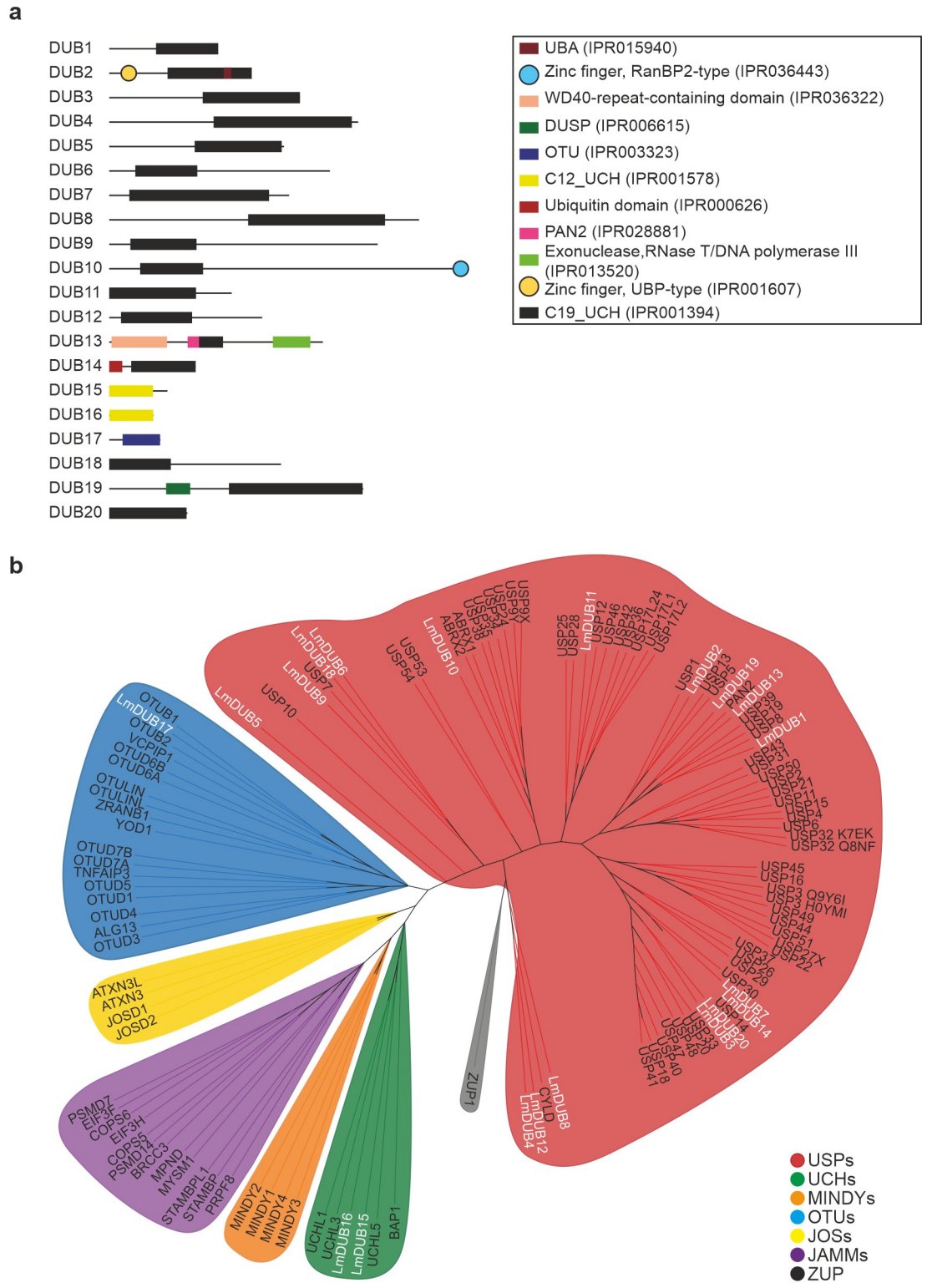
Fig 1. *Leishmania* DUBs domain analysis and phylogenetic tree. (A) Domain analysis of 20 predicted cysteine peptidase DUBs. InterPro was used to analyse protein sequences. Identified domains, including their InterPro entry code, are shown. (B) Phylogenetic tree for the deubiquitinase domains of *L. mexicana* and *H. sapiens* DUBs. UBA; ubiquitin associated, DUSP; domain present in ubiquitin-specific proteases, OTU; ovarian tumour, UCH; ubiquitin C-terminal hydrolase, PAN; poly(A)-specific nuclease, USP; ubiquitin-specific protease, UCH; Ubiquitin carboxyl-terminal hydrolase, MINDY; Motif interacting with ubiquitin-containing novel DUB family, JOS; Josephin domain-containing, JAMM; Jab1/Mov34/Mpr1, ZUP; Zinc finger-containing ubiquitin peptidase.

https://doi.org/10.1371/journal.ppat.1008455.g001

Table (panel c):

Name	Null Mutant			F. Null mutant	Mass Spe.
	1st	2nd	3rd		
DUB1	🔴	🔴	🔴	🟢	
DUB2	🔴	🔴	🔴	🟢	🟢
DUB3	🟢				🔴
DUB4	🔴	🟢			🔴
DUB5	🟢				🔴
DUB6	🔴	🔴	🟢		🔴
DUB7	🟢				🔴
DUB8	🟢				🔴
DUB9	🟢				🔴
DUB10	🟢				🔴
DUB11	🟢				🔴
DUB12	🔴	🔴	🔴	🟢	🔴
DUB13	🔴	🟢			🔴
DUB14	🟢				🔴
DUB15	🟢				🔴
DUB16	🔴	🔴	🔴	🟢	🟢
DUB17	🟢				🔴
DUB18	🟢				🟢
DUB19	🟢				🟢
DUB20	🟢				🔴

🟢 Success/Detected   🔴 Fail/Not Detected
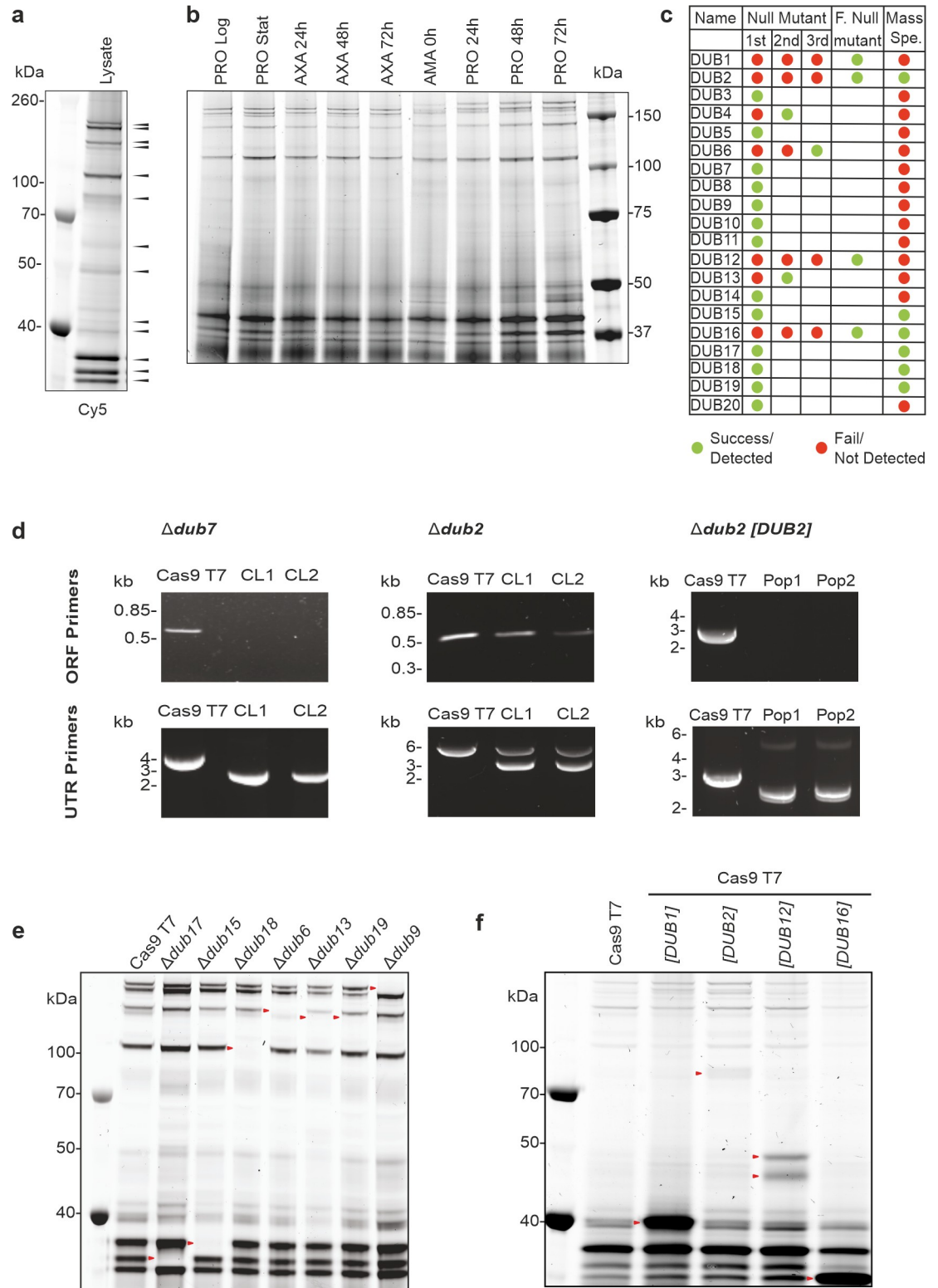
Fig 2. Validation of DUB null mutants. (A) DUB activity in *L. mexicana* promastigote cell lysates was profiled using Cy5UbPRG. Proteins were resolved by SDS-PAGE and in-gel fluorescence (Cy5) was captured using a Typhoon imager. Black arrows represent the higher intensity activities. (B) DUB activity profiled using Cy5UbPRG in log phase promastigotes (PRO Log), stationary phase promastigotes (PRO Stat), axenic amastigotes (AXA) grown for 24, 48 and 72 h after differentiation from stationary phase promastigotes, lesion-derived amastigotes (AMA) and promastigotes 24, 48 and 72 h after differentiation from AMA. (C)

Summary of null mutant generation and isolation of DUBs by affinity purification. Green, successful; red, not successful. F., facilitated; Spe., spectrometry. (D) Example of diagnostic PCRs performed to confirm a null mutant for a non-essential gene (Δ*dub7*), a heterozygote for an essential gene (Δ*dub2*) and the generation of a facilitated null mutant (Δ*dub2 [DUB2]*). (E) DUB activity profiling of lysate extracted from null mutant lines of log-phase *L. mexicana* promastigotes. Arrowheads represent the absence of an active DUB compared to the Cas9 T7 parental cell line. (F) DUB activity profiling of lysate extracted from facilitated null mutant lines of log-phase *L. mexicana* promastigotes. The arrow heads represent the DUB expressed from the episome.

round of transfection into the parental *L. mex* Cas9 T7 line, two independent null mutant lines were generated for 13 DUBs (Δ*dub3*, Δ*dub5*, Δ*dub7*, Δ*dub8*, Δ*dub9*, Δ*dub10*, Δ*dub11*, Δ*dub14*, Δ*dub15*, Δ*dub17*, Δ*dub18*, Δ*dub19*, Δ*dub20*) and validated using PCR to detect correct integration of the resistance cassettes and removal of the open reading frame (Fig 2D, S2 Fig and S3 Table). After further transfections, another 3 null mutants were isolated (Δ*dub4*, Δ*dub6* and Δ*dub13*), making a total of 16. For four DUBs, *DUB1*, *DUB2*, *DUB12* and *DUB16*, null mutants could not be generated.

To identify the DUB activities detected in promastigotes (Fig 2A), cell lysates for the *DUB* null mutants were probed with the Cy5UbPRG ABP (Fig 2E, S3 Fig), with the expectation that the absence of a band of activity in comparison to the *L. mexicana Cas9* T7 would represent the DUB that had been deleted. This allowed us to identify 5 active DUBs close to their expected sizes; DUB6 (133 kDa), DUB9 (155 kDa), DUB15 (34 kDa), DUB17 (30 kDa) and DUB18 (102 kDa). The fact that DUB15, DUB16, DUB17, DUB18, and DUB19 had been affinity purified with the UbPRG probe shows that these DUBs are active in the promastigote stage. A similar-sized DUB activity present in *L. mexicana* Cas9 T7 was absent in promastigotes of both Δ*dub13* and Δ*dub19*, but we were unable to identify the DUB. Of note, PAN2, the human orthologue of DUB13, does not appear to bind the Cy5UbPRG probe [24], as it lacks key catalytic residues including the active Cys. This may also be true for *L. mexicana* DUB13.

To investigate further, promastigote cell lines were differentiated to amastigotes and probed with the ABP. This allowed DUB8 (172kDa) and DUB19 (148kDa) to be identified by comparing wild type and Δ*dub8* and Δ*dub19* (S3D Fig). Several null mutant DUB cell lines did not show any depletion of activity with the Cy5UbPRG profiling in either promastigotes or amastigotes, suggesting that those DUBs are not expressed, not active or are below detection limits of the ABP in the promastigote stage under the environmental conditions tested. Alternatively, the DUBs may not bind the ABP.

It was not possible to isolate null mutant clones for *DUB1*, *DUB2*, *DUB12* and *DUB16*, possibly because those DUBs are essential in promastigotes (Fig 2C). In three instances (*DUB1*, *DUB2* and *DUB12*), correct integration of the drug resistance cassettes was observed, but the parasites retained a wild type copy of the gene, indicating that the genes are essential (S2 Fig). For *DUB16*, no populations could be recovered after the transfections. To provide further evidence that the genes are essential and to discount the possibility that the lack of gene deletion was a technical failure, facilitated null mutants were generated for the four *DUB* genes. Initially, the parental Cas9 T7 cell line was transfected with a plasmid expressing the DUB, thereafter the two alleles in the genomic locus were deleted successfully using CRISPR, two independent populations isolated, and the expected gene editing confirmed by diagnostic PCR (Fig 2D and S2C Fig). The Cy5UbPRG ABP was used to identify the over-expressed and active DUBs in the *L. mexicana* Cas9 T7 [*DUB*] cell lines (Fig 2F), where an increase in specific activities were detected in the over-expression lines compared to the parental line (Fig 2F, arrow heads). For DUB2 and DUB16 the expected sizes of 81 and 25 kDa were detected respectively, once the ~9 kDa mass of the ABP had been taken into account. In contrast, both DUB1 (expected size 65 kDa, observed size 40 kDa) and DUB12 (expected size 89 kDa, observed sizes

45 and 50 kDa) are smaller than expected and seem likely to be proteolytically processed in the cell (Fig 2F).

Bar-seq reveals the importance of DUBs in the *L. mexicana* life cycle

To assess the ability of the DUB null mutants to transition through the parasite life cycle, bar-seq analysis, a method that involves the parallel phenotyping of pools of mutants using high-throughput DNA sequencing, was carried out [25]. Our 58 barcoded null mutants representing 16 DUBs, 13 other peptidases, 25 other ubiquitination system genes and 4 protein kinases (S4 Table) were prepared in equal proportions in 6 replicate promastigote (PRO) pools. The pools were grown for 7 days (d) before samples were collected and either induced to form axenic amastigotes (AXA) or used to purify metacyclic stage promastigotes (META). Purified metacyclic promastigotes were used to infect macrophages (inMAC) *in vitro* or mice via footpad (FP) injection. At various time points, DNA samples were prepared from the pool for amplification of the barcodes by PCR and quantitative analysis via next generation sequencing (Fig 3A, S4 Table).

In order to analyse fitness, defined as *"the reproductive capacity of a given population in a given environment"* the number of reads for each barcode was first divided by the total number of reads for expected barcodes at each experimental stage. Next, data were averaged across the 6 replicates and the barcodes matched back to their respective null mutant lines. Changes in the average proportional representation of these lines were then used to infer changes in fitness. Importantly, because of the potential for the cumulative loss of null mutant lines during the experiment, statistical tests to investigate loss of fitness were only applied between adjacent time points. This ensured that the experimental period linked with a particular viability defect could be identified. Additionally, because of the higher likelihood that null mutant lines would exhibit decreased, rather than increased, fitness during the experiment (leading to an overall increase in the proportional representation of remaining null mutant lines), increases in fitness could not be confidently reported. Consequently, our analysis focuses only on deficiencies in life cycle progression.

Barcodes were detected for all null mutant lines at time point zero, however, very few reads were found for *Δdub18* (most likely due to experimental error), leading this null mutant line to be excluded from the analysis. Decreased fitness was observed between adjacent promastigote stages (PRO 0 h-PRO 168 h) for a number of null mutant lines, with *Δdub8*, *Δdub9* and *Δdub13* in particular showing reduced fitness at two promastigote time points (unpaired t-tests with Holm- Šídák correction for multiple comparisons, $p<0.05$). None of the mutants had significantly decreased fitness between the 168 h and metacyclic promastigote (META) samples, however, strong loss of fitness was common upon entering the amastigote life cycles stages (AXA 24 h onwards, inMAC 12 h onwards and FP 3 onwards, Fig 3B–3D respectively). Strong defects in both axenic amastigote differentiation and macrophage infection were observed for *Δdub4*, *Δdub7* and *Δdub13* (≥85-fold, ≥7-fold and ≥50-fold decreases in fitness respectively). Additionally, decreased fitness was observed for *Δdub5*, *Δdub8*, *Δdub9*, *Δdub10* and *Δdub11* between the AXA 24 h and AXA 120h stages and for *Δdub6*, *Δdub11* and *Δdub17* between the META and inMAC 12 h stages. Consistent with their phenotypes in axenic amastigotes, *Δdub4*, *Δdub7* and *Δdub13* showed severe reductions (to zero) in fitness during mouse infection. Additional defects of 20-fold or more reduction in fitness were also seen for *Δdub3*, *Δdub5*, *Δdub6*, *Δdub8*, *Δdub10*, *Δdub11* and *Δdub14*. While many examples of loss of fitness in mouse infection were observed for DUBs and other ubiquitination system mutants studied (S4 Table), loss of fitness phenotypes were less common for other peptidase mutants in the screen,
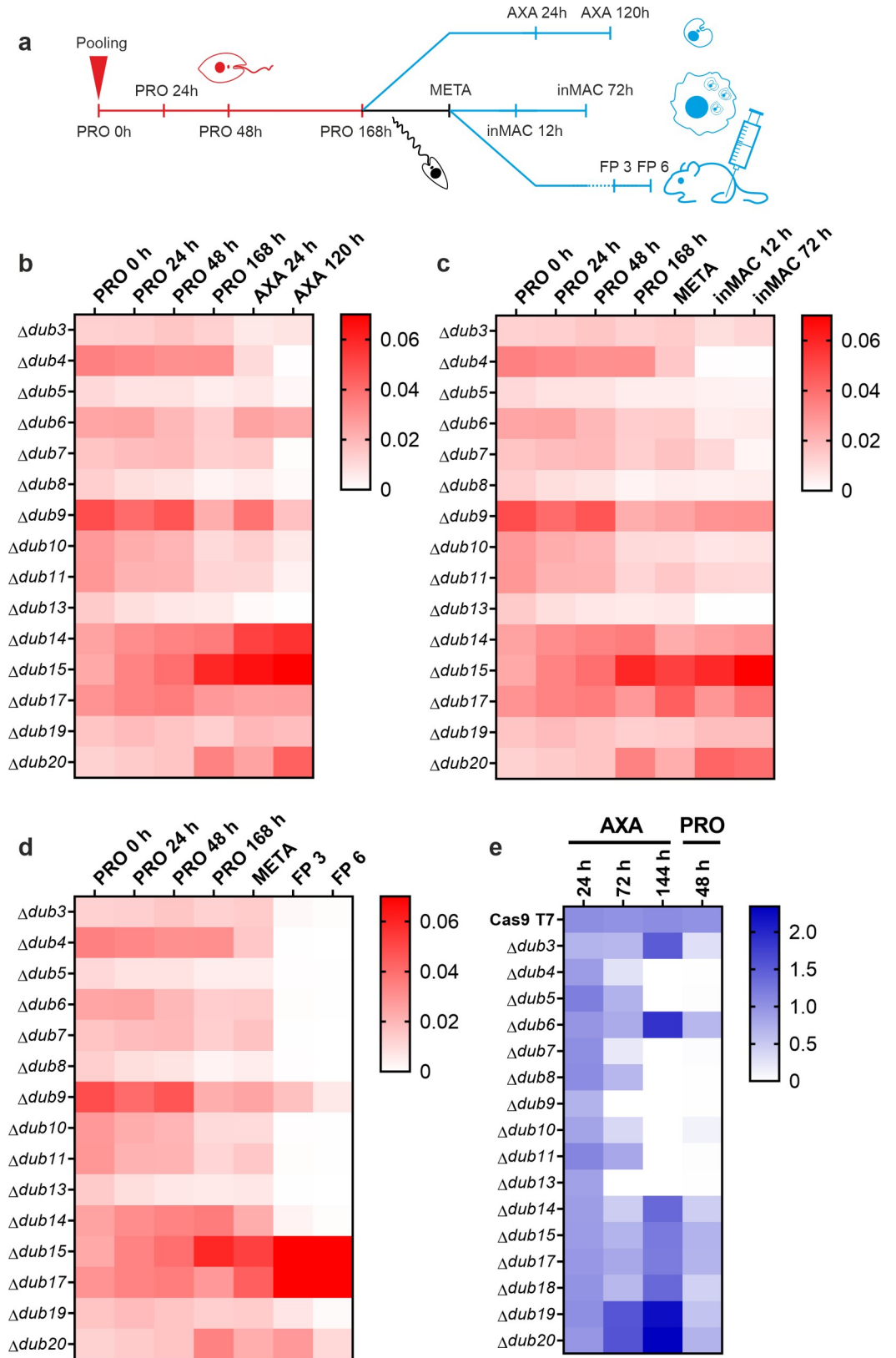
Fig 3. Life cycle phenotyping of DUB null mutants by bar-seq. Fifty-eight null mutants were pooled (n = 6) as promastigotes and grown to stationary phase before being induced to differentiate to axenic amastigotes *in vitro* or used for

metacyclic purification and subsequent infection of macrophages or mice. At the time points indicated in (A), DNA samples were extracted for barcode amplification by PCR and quantitative analysis by next generation sequencing. Average proportional representation of null mutant-specific barcodes at each experimental stage is displayed in the heat maps for (B) axenic amastigote, (C) macrophage infection and (D) mouse infection experiments. Samples included represent promastigote time-point zero (PRO 0 h), early-log phase (PRO 24 h), mid-log phase (PRO 48 h), late-log phase (PRO 72 h), stationary phase (PRO 168 h), early axenic amastigote differentiation (AXA 24 h), post-axenic amastigote differentiation (AXA 120 h), purified metacyclic promastigotes (META), early macrophage infection (inMAC 12 h), late macrophage infection (inMAC 72 h), 3 week footpad mouse infection (FP 3) and 6 week footpad mouse infection (FP 6). Separately, individual null mutant lines were grown to stationary phase and induced to differentiate into axenic amastigotes. Cell viability was measured at the stages indicated in (E) using resazurin (added 24 h prior to each measurement). A transformation step back to promastigotes was included. Measurements of cell viability were calculated relative to the wild-type at each experimental stage. The data are an average of two independent experiments.

including members of the calpain (C2), SUMO-specific peptidase (C97) and D-alanyl-glycyl endopeptidase (C51) families [26].

To demonstrate the validity of the phenotypes observed in the bar-seq screen, null mutants were also analysed individually at 24, 72 and 144 h after induction of amastigote differentiation and 48 h after transformation of axenic amastigotes back to promastigotes using resazurin, an oxidation-reduction indicator that reports on cell activity. The data from this experiment match well with the phenotypes observed in the AXA bar-seq data (Fig 3E). An exception to this is Δ*dub9* which is well represented throughout the bar-seq experiment but loses viability at 72 h in the cellular assay, perhaps indicating the persistence of Δ*dub9* beyond 72 h but in a metabolically inactive state. The viability data also support more unusual phenotypes. For example, Δ*dub6* is still well represented at the AXA 24 h and 120 h stages of the bar-seq experiment but less so at the inMAC 12 h stage. This is supported by data from the viability assay showing that Δ*dub6* is viable throughout amastigote differentiation. Based on this finding, one could hypothesise that DUB6 may contribute to part of the infection process such as parasite entry into macrophages or survival in the phagolysosomes. Overall, the phenotypes observed in the pooled context of the bar-seq experiment reflect well the individual phenotyping of the viability assay. To further validate how these null mutants behave during amastigote differentiation, a western blot against HASPB, a marker for amastigotes [27], was performed. Δ*dub4*, Δ*dub7*, Δ*dub9* and Δ*dub13* showed very low or no expression of HASPB 120 h after the initiation of differentiation (S3 Fig). These results further demonstrate the inability of Δ*dub4*, Δ*dub7*, Δ*dub9*, and Δ*dub13* to differentiate into amastigotes (first shown in Fig 3E).

DUB2 activity is essential for *L. mexicana*

L. mexicana DUB2 is one of the four essential DUBs identified in the CRISPR-Cas9 screen and is classified as a member of the USP family, closely related to mammalian USP5, USP13 and USP1 (Fig 1B). DUB2 domain analysis suggested the presence of a peptidase C19, ubiquitin carboxyl-terminal hydrolase domain, a UBA (ubiquitin-associated domain and a Zinc finger UBP-type) (Fig 1A). The UBA domain found in the C-terminal end of DUB2 is present in many proteins associated with the ubiquitin system, and it is responsible for the binding of ubiquitinated substrates [28]. The Zinc finger domain is found only in a minor subfamily of USP DUBs including the mammalian USP5, USP13 and USP39, regulators of deubiquitination [18].

A modified version of the inducible DiCre system [29] was applied to *L. mexicana DUB2* to investigate its function in promastigotes. The first allele of *DUB2* was replaced with a *DUB2* flanked by LoxP sites (Δ*dub2*::*DUB2*^FLOX^/*DUB2*, called DUB2^+/+FLOX^). Subsequently, the second allele of *DUB2* was replaced with a *HYG* resistance cassette (Δ*dub2*::*HYG*/Δ*dub2*::*DUB2*-^FLOX^, called *DUB2*^-/+FLOX^). The expected genetic modifications for several clones were

confirmed by PCR (S5A Fig). Excision of *DUB2* in *DUB2*$^{+/+FLOX}$ and *DUB2*$^{-/+FLOX}$ logarithmic phase promastigotes was confirmed by the PCR amplification of a 1.3 kb DNA fragment in only those cells treated with 100 nM rapamycin (Fig 4A). A pronounced defect in cell growth was observed in the rapamycin treated DUB2$^{-/+FLOX}$ cell line in comparison to DUB2$^{+/+FLOX}$ or untreated controls, indicating that deletion of both *DUB2* alleles is required to elicit a growth phenotype (Fig 4B). The Cy5UbPRG ABP demonstrated that the activity of DUB2 sharply decreased in the induced DUB2$^{-/+FLOX}$ line, but not in DUB2$^{+/+FLOX}$ or WT (Fig 4C). For further analysis, the in-gel fluorescence band intensity was quantified for the DUB2$^{-/+FLOX}$ line, showing one band (band 9) had a 70% depletion after rapamycin induction (Fig 4D). Band 9 is the same size as that observed in the episomal over-expression of DUB2 (Fig 2E) and correlates with the predicted mass of DUB2 protein covalently bound to the ABP (~100 kDa). A second unidentified DUB, labelled Unk 4, had a slight increase in activity after depletion of DUB2 in the DUB2$^{-/+flox}$ line (Fig 4C and 4D). Loss of DUB2 may cause a compensatory change in activity for this DUB.

To confirm that the depletion of DUB2 leads to cell death a clonogenic assay was performed on *DUB2*$^{+/+FLOX}$ and *DUB2*$^{-/+FLOX}$ promastigotes following treatment with rapamycin or DMSO for 48 h. A >90% decrease in numbers of clones surviving for both *DUB2*$^{-/+FLOX}$ clones was observed for cells treated with rapamycin, whilst there was no difference in the number of clones surviving in the *DUB2*$^{+/+FLOX}$ line, despite the presence of rapamycin (Fig 4E). These data confirm that the loss of *DUB2* leads to death of promastigotes and that one allele of *DUB2* can sustain growth. Finally, diagnostic PCR confirmed the presence of *DUB2* in *DUB2*$^{-/+FLOX}$ cells that survived rapamycin treatment, showing that if *DUB2* is deleted, the cells were non-viable (S5B Fig). In support of these observations a significant increase in cell death was observed using propidium iodide staining after induction (S5C Fig).

Alignment of the C19 domain of DUB2 with other DUBs allowed the identification of C312 as the likely active site Cys. A point mutation was introduced into *DUB2* in a pNUS plasmid to change the encoded Cys 312 to alanine, which would result in abolishment of DUB2 activity. pNUS-*DUB2* and pNUS-*DUB2*^{C312A} plasmids were transfected into *DUB2*$^{-/+FLOX}$ and an ABP assay with Cy5UbPRG used to confirm an increase of DUB2 activity in *DUB2*$^{-/+FLOX}$ [DUB2] but not *DUB2*$^{-/+FLOX}$ [DUB2^{C312A}] (Fig 4F). Over-expression of DUB2 was confirmed in both *DUB2*$^{-/+FLOX}$ [DUB2] and *DUB2*$^{-/+FLOX}$ [DUB2^{C312A}] cell lines by western blot using an antibody raised against *T. brucei* DUB2; this cross-reacts with *L. mexicana* DUB2 (Fig 4G). These data confirm that C312 is the active site Cys and is required for DUB2 activity. The loss of the *DUB2* following rapamycin treatment resulted in a 90% decrease in the number of *DUB2*$^{-/+FLOX}$ [DUB2^{C312A}] clones in comparison to *DUB2*$^{-/+FLOX}$ [DUB2] (Fig 4E); indeed, expression of DUB2 in the *DUB2*$^{-/+FLOX}$ line resulted in full complementation of the cell death phenotype. Taken together, these experiments strongly support that the deubiquitinase activity of DUB2 is required for the survival of *L. mexicana* promastigotes.

The *DUB2*$^{-/+FLOX}$ line was also used to examine if *DUB2* is essential for infection and survival in BALB/c mice. Mid-log phase WT and *DUB2*$^{-/+FLOX}$ were grown in the presence or absence of rapamycin for 72 h and then inoculated into BALB/c mice. Efficient excision of DUB2 was confirmed by PCR (Fig 5A). The mice infected with the rapamycin-treated WT or non-treated *DUB2*$^{-/+FLOX}$ showed a steady growth in footpad size whereas rapamycin-treated mice *DUB2*$^{-/+FLOX}$ did not develop a footpad lesion (Fig 5B), had 100-fold less parasites than non-treated in the footpad and could not be detected in the popliteal draining lymph nodes (Fig 5C). The presence of a small number of parasites in the footpad of treated mice might be due to the presence of a subpopulation of cells that retained the floxed *DUB2*. This was supported by the finding that DUB2 could be detected by PCR in cells isolated from treated
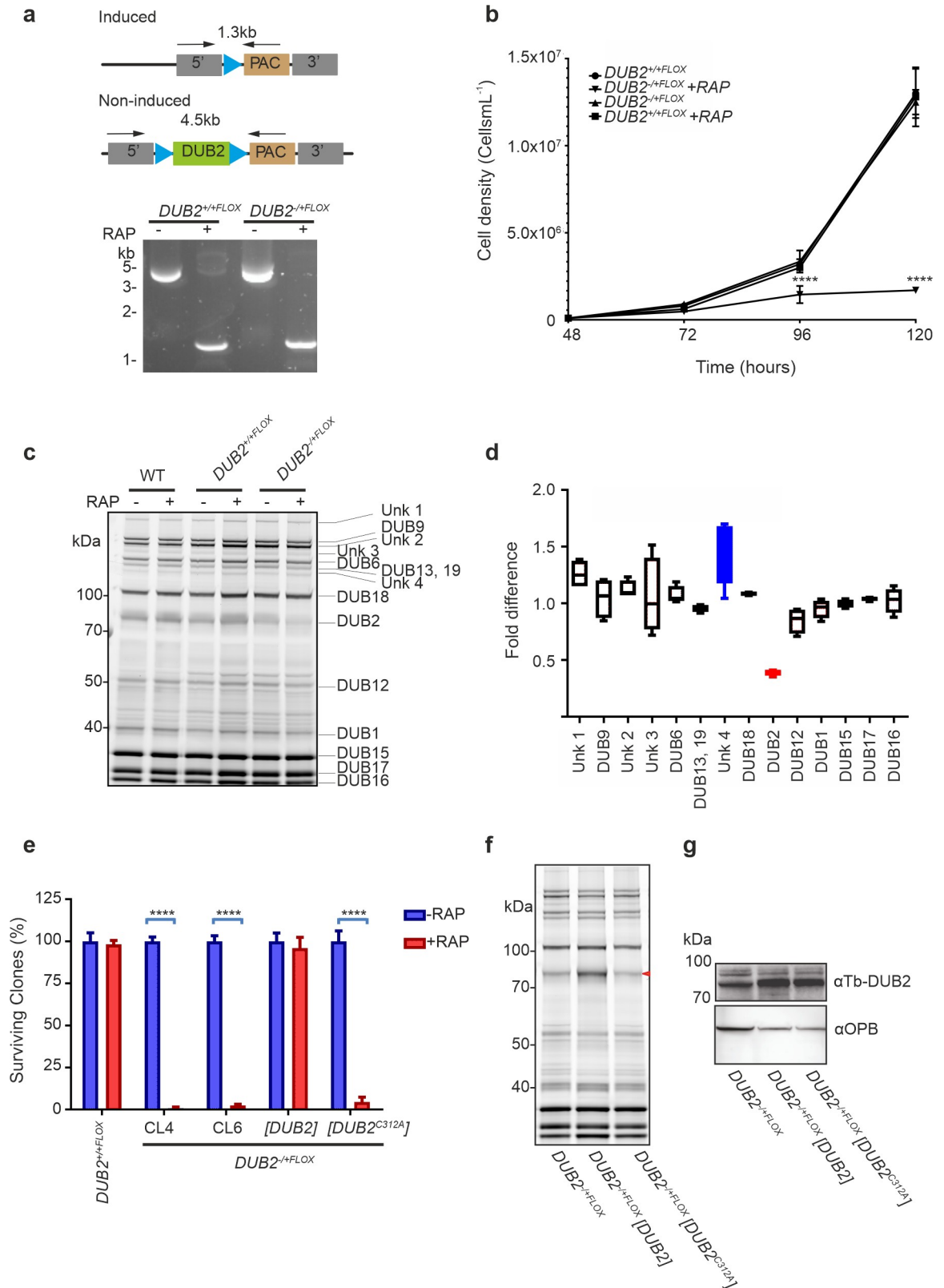
Fig 4. Conditional deletion of *DUB2*. (A) (Top) Schematic representation of the loxP-flanked *DUB2* allele before and after rapamycin-induced recombination by DiCre. Arrows represent the primers used for the PCR to check for the successful excision of *DUB2*. (Bottom)
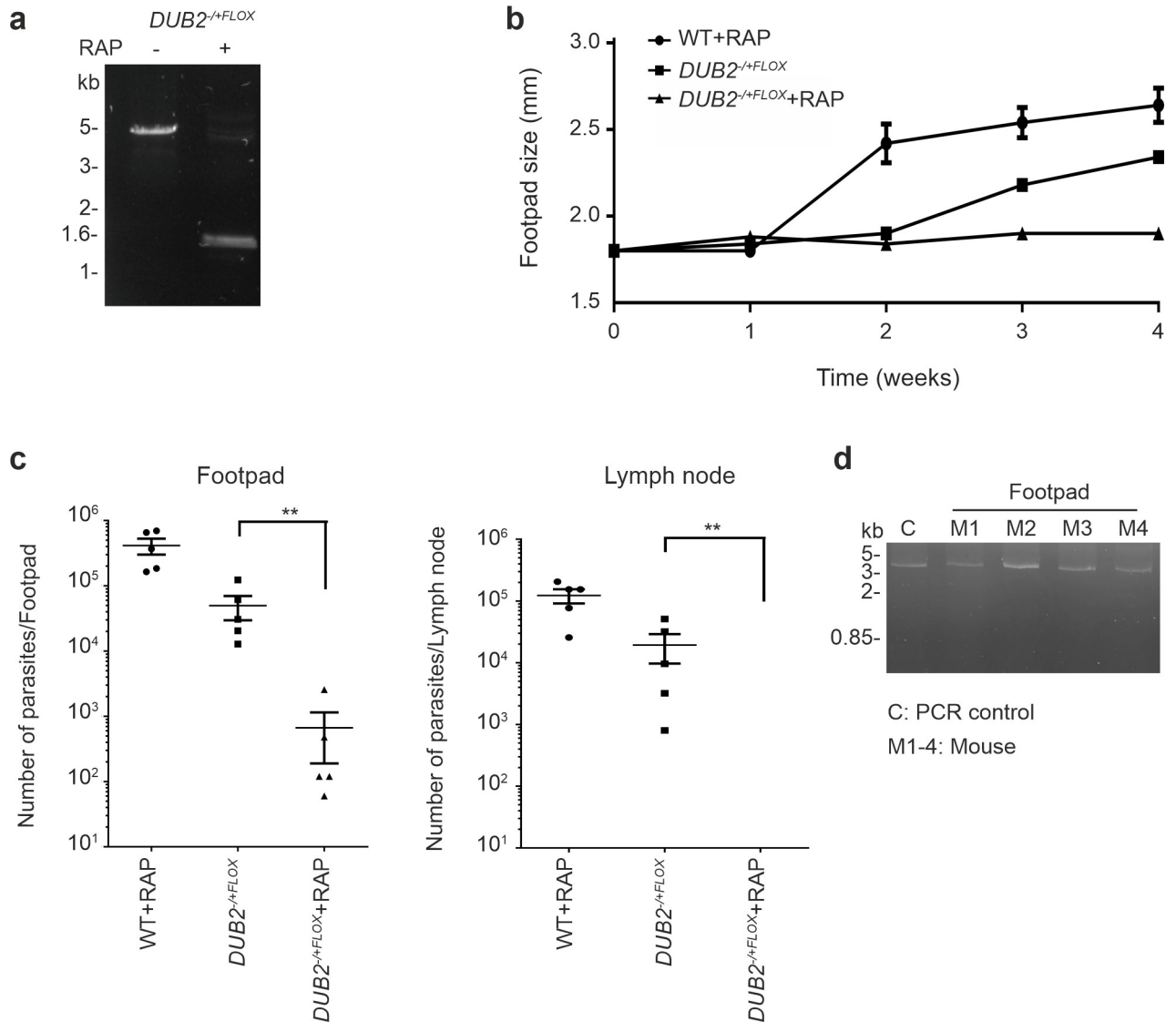
PCR amplification of *DUB2*$^{+/+FLOX}$ and *DUB2*$^{-/+FLOX}$ +/- 100 nM RAP for 48 hours was conducted and the resulting amplicons resolved on 1% agarose gel stain with SYBR safe. (B) *DUB2*$^{+/+FLOX}$ and *DUB2*$^{-/+FLOX}$ promastigotes were seeded at a density of 1×10^5 cells mL^{-1} and grown in the absence or presence (-/+) of 100 nM RAP for 48 h. Cells were diluted to 1×10^5 cells mL^{-1} and allowed to grow in the presence or absence of 100 nM RAP for 4 d. Cell density was determined by counting at 24 h intervals and mean ± SD of triplicate values were plotted. The data were analysed in Prism software, and an unpaired t-test performed to indicate the significance (n = 5) between different time points, comparing treated with RAP to untreated samples. Error bars show the standard deviation of the mean. ****p < 0.0001. (C) DUBs visualised by in-gel fluorescence analysis after separation by SDS PAGE. Samples were lysed, and 25 μg of lysate was incubated with the probe for 30 min. The positions of the different DUBs are indicated. (D) Fold difference of the DUB activity comparing *DUB2* induced/*DUB2* non-induced of the *DUB2*$^{-/+FLOX}$, data from (C). Band intensities were quantified by densitometry using GelAnalyzer 19.1 software. Each band is represented as a percentage of the total activity. The percentages for each band for the induced sample were divided by the non-induced to determine the fold difference. The data were then analysed in Prism software. Each column represents the mean of data from three independent experiments. Error bars show the standard deviation of the mean. Blue represents an increase of more than 1.3-fold whereas red represents a difference of less than 0.7-fold. (E) Percentage of surviving clones of *DUB2*$^{+/+FLOX}$, *DUB2*$^{-/+FLOX}$ clone 4, *DUB2*$^{-/+FLOX}$ clone 6, *DUB2*$^{-/+FLOX}$ [*DUB2*] and *DUB2*$^{-/+FLOX}$ [*DUB2*^{C312A}] promastigotes after RAP induction. The cell lines were incubated with or without RAP for 48 hours. Next, cells were counted and cloned into 96 well plates. After 4 weeks, plates were checked for surviving parasites. The data were then collected and analysed in Prism software. 100% represents the highest number of surviving parasites that were collected from an individual experiment in the absence of RAP. Each column represents the mean of data from three independent experiments. Error bars show the standard deviation of the mean. ****p < 0.0001. (F) DUBs were visualised by in-gel fluorescence analysis after separation by SDS-PAGE. Samples were lysed and 25 μg of lysate was incubated with the probe for 30 min. Lysate was collected from *DUB2*$^{-/+FLOX}$, *DUB2*$^{-/+FLOX}$ [*DUB2*] and *DUB2*$^{-/+FLOX}$ [*DUB2*^{C312A}] promastigotes grown in the presence of 10 μg μL^{-1} of G418. (G) Western blotting analysis with anti-TbDUB2 (1:1,000) and anti-LmOPB (1:20,000) (loading control) antibodies on protein extracted from *DUB2*$^{-/+FLOX}$, *DUB2*$^{-/+FLOX}$ [*DUB2*] and *DUB2*$^{-/+FLOX}$ [*DUB2*^{C312A}] promastigotes grown in the presence of 10 μg μL^{-1} of G418.

DUB2$^{-/+FLOX}$ lesions (Fig 5D). In summary, *DUB2* is required either for the establishment and/or maintenance of an infection in mice.

The DUB2 interactome

To gain more insight into the function of DUB2, the DUB2 interactome was investigated. The expression of active N-terminally tagged 3 x myc mNeo DUB2 was confirmed with the ABP and Western blotting (S6 Fig). DUB2 and an N-terminally tagged 3 x myc mNeo RDK2 control were immuno-precipitated from *L. mexicana* promastigote cell lysates and proteins identified by mass spectrometry. Parasites were cross-linked with dithiobis(succinimidyl propionate) to enable transient interactors to be captured, including possible substrates of DUB2. In the DUB2 samples, a total of 1269 protein groups were identified across 3 independent replicates, of these 818 were commonly identified in all three DUB2 replicates. Data were processed with an interaction scoring algorithm SAINTq to provide a score on the probability of a true interaction with DUB2. This analysis produced a list of 110 high confidence DUB2 interactors at <1% FDR (Fig 6, S5 Table). The list includes a number of proteins involved in ubiquitination, including polyubiquitin, three putative E2 ubiquitin-conjugating enzymes (*LmxM.34.1300*, *LmxM.04.0680*, *LmxM.13.1580*) and an ubiquitin-like modifier peptidase (*LmxM.32.2260*). Among the most enriched proteins was CYC12 (*LmxM.36.5640*), an L-type cyclin involved in spliced leader trans-splicing of pre-mRNA [30]. Other proteins involved in mRNA splicing were also enriched including SmD2, U5 snRNP and snRNP-B. Three members of the cleavage and polyadenylation specificity factor complex (CPSF) and a cleavage stimulation factor co-purified, suggesting a role for DUB2 in the processing of mRNA. Proteins involved in mRNA capping, CBP110 and CGM1, were also strongly enriched with DUB2. In addition, 19 of the interactors are either annotated as RNA binding or known to have a role in RNA metabolism. A smaller number of DUB2 interactors are implicated in transcription, however, this group includes the top enriched interactor NIF3. Interestingly, among this group of proteins involved in transcription/chromatin dynamics is Nucleosome Assembly Protein, NAP, which was enriched 27-fold. In humans, NAP1 is a histone chaperone and plays an important role in nucleosome assembly/disassembly by binding to free H2A/H2B dimers

Fig 5. *In vivo* characterisation of *DUB2*. (A) PCR amplification of the floxed *DUB2* locus of *DUB2*$^{-/+FLOX}$ of 4 x 10^6 cells mL^{-1} log phase promastigotes after incubation in the presence (+) or absence (-) of 1 μM RAP for 72 h. The resulting amplicons were resolved in 1% agarose gel stain by SYBR safe. Schematic representation of the primers used for the PCR, as well as the expected fragments (4.5 kb, 1.3 kb), are shown in Fig 4A. (B) Mice were infected in the footpad with 2 x 10^6 WT+RAP, DUB2$^{-/+FLOX}$ and DUB2$^{-/+FLOX}$+RAP promastigotes and footpad size was recorded by weekly caliper measurement. Data were analysed in Prism software. Data shown represent the mean footpad size and SD from groups of five mice. (C) Parasite burden. Mice were sacrificed after 4 weeks, and parasite loads in footpad and popliteal lymph node were determined by limiting dilution. Statistical analyses were performed in Prism software using the paired t-test. (D) PCR amplification to check *DUB2* excision of the samples collected from the mice which were infected with the *DUB2*$^{-/+FLOX}$ +RAP. The resulting amplicons were resolved in 1% agarose gel stained with SYBR safe. Schematic representation of the primers used for the PCR, as well as the expected fragments (5.6 kb, 1.3 kb), are shown in Fig 4A.

[31]. Cycles of ubiquitination and de-ubiquitination of H2B are well known to play an important role in nucleosome dynamics during transcription and DNA replication. Several proteins with key roles in DNA replication were also identified as DUB2 interactors, such as PCNA, DNA polymerase delta and subunits of replication factor A and C. In other organisms, multiple components of the DNA replication machinery are ubiquitinated, in particular, ubiquitination of PCNA is critical for recruitment of DNA polymerases [32]. The identification of VPS4 [33] and a dynamin-1 like protein suggest involvement of DUB2 in endosomal trafficking.
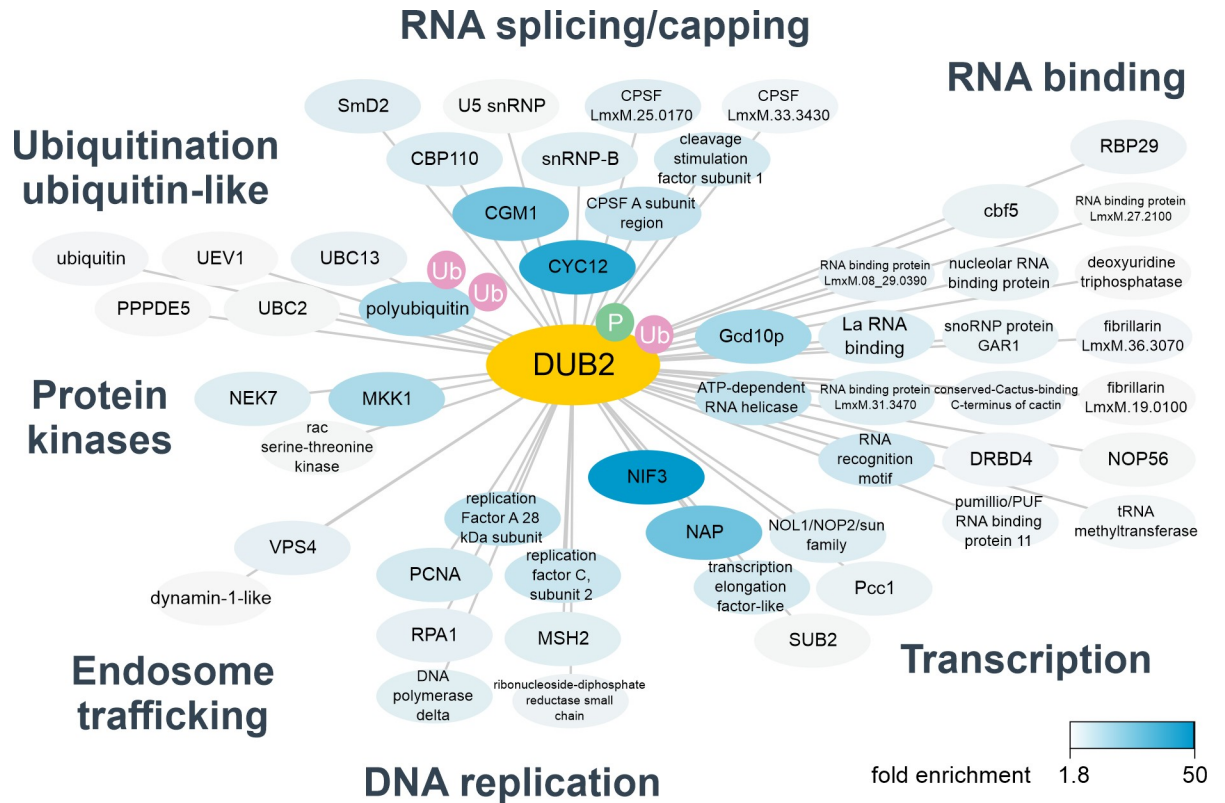
Fig 6. DUB2 interactome. Summary of detected DUB2 interactions. Myc-DUB2 was immuno-precipitated from promastigotes and binding partners identified by label free quantitative mass spectrometry. Interaction data were analysed with SAINTq, high confidence interactors (<1% FDR) were selected and are shaded according to fold enrichment against a control immuno-precipitation. Detected ubiquitination sites (Ub) and phosphorylation (P) are shown. Interactors are grouped according to the annotated function. A total of 110 high confidence interactors were identified. Non-annotated or ribosomal proteins have been omitted for clarity.

https://doi.org/10.1371/journal.ppat.1008455.g006

Finally, 3 protein kinases were co-enriched, including a mitogen activated protein kinase kinase (MKK1). This suggests a mechanism of DUB2 regulation, therefore mass spectrometry data were searched for phosphorylation sites revealing that DUB2 is phosphorylated on a serine in the region 586–589. A ubiquitination site in DUB2, K681, was also identified suggesting that DUB2 itself may be regulated by the ubiquitination pathway (S6 Table). Overall, the multiple interactions of DUB2 with splicing factors, proteins involved in mRNA capping and factors regulating chromatin dynamics/transcription, place DUB2 near actively transcribing genes.

DUB2 has deubiquitinating activity

To explore the function of DUB2 in more detail, recombinant enzyme (DUB2) and a catalytically inactive form (DUB2^{C312A}) were expressed and purified using a baculovirus insect cell expression system (S7 Fig). DUB2, but not DUB2^{C312A} recombinant protein reacted with the Cy5UbPRG probe (Fig 7A) and 85% of the recombinant DUB2 reacted with the probe (Fig 7B). DUB2 linkage specificity against all eight types of human di-ubiquitin was then investigated over 30 min at a constant enzyme and substrate concentration. At 0.02 nM DUB2 had a preference for cleavage at Lys-11, Lys-29, Lys-33 and Lys-63, but at 2 nM DUB2 cleaved all linkages except Lys-27 (Fig 7C). Finally, DUB2, but not DUB2^{C312A} recombinant protein had activity towards Ub-AMC substrate with a k_{cat} of 0.049 s^{-1} and a K_m of 14.9 x 10^{-6} M (Fig 7D).
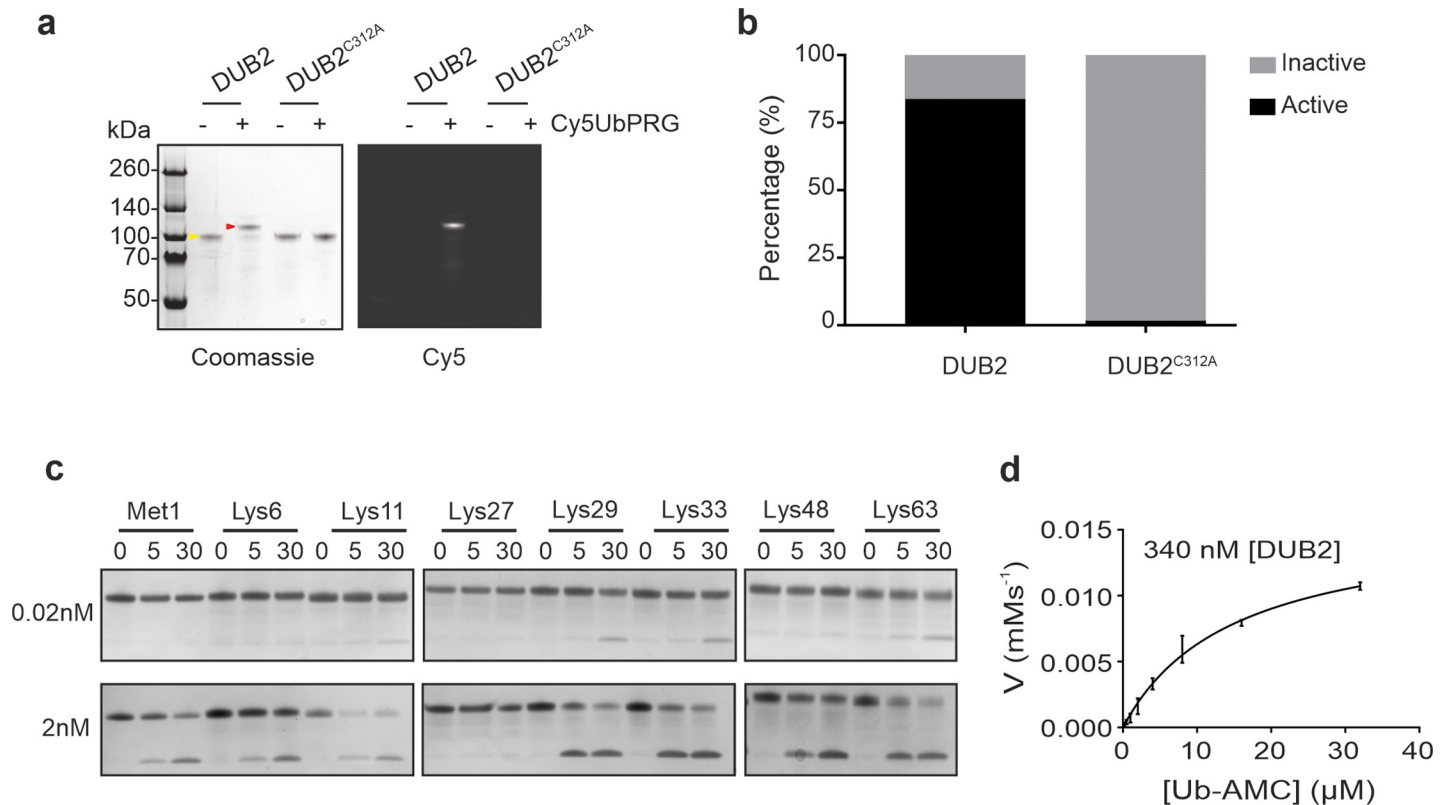
Fig 7. *In vitro* characterization of DUB2 recombinant protein. (A) 500 ng of purified DUB2 and DUB2[C312A] were incubated with or without 1.2 μg of Cy5UbPRG for 30 min. Samples were analysed by SDS-PAGE gel electrophoresis with in-gel fluorescence (Cy5). The gel was stained in InstantBlue protein stain. The yellow arrowhead indicates DUB2 and the red arrowhead shows DUB2 in complex with the Cy5UbPRG probe. (B) The stained gel in (A) was analysed using GelAnalyzer 19.1 software to determine the band intensity for DUB2 and DUB2 in complex with the ABP. Data were then collected and analysed to determine the ratio between the active and inactive form of DUB2 in Prism software. (C) Different di-ubiquitin linkage types were incubated with recombinant DUB2 (0.02 nM or 2 nM) for the times indicated and proteins resolved by SDS-PAGE gel and stained with InstantBlue Protein Stain. (D) Michaelis-Menten kinetic analysis for DUB2 hydrolysis of Ub-AMC. Error bars represent s.d. from the mean. Reactions containing 400 nM DUB2 were initiated by the addition of Ub-AMC at final concentrations between 0.25 μM and 32 μM. Assays were performed in triplicate for three independent experiments. Initial rates were determined by calculating the gradient of a linear regression of the product concentration against time (from 0–400 sec).

Discussion

Recent studies showed the potential for proteasome inhibition as a treatment for three diseases caused by trypanosomatid parasitic protozoa, including leishmaniasis [9, 10]. The proteasome is dependent on the ubiquitination pathway to identify substrates for degradation and a search of the *Leishmania* genome reveals a range of E1, E2 and E3 ligases, as well as a number of DUBs [34]. Nevertheless, there have been no extensive studies exploring the role and essentiality of *Leishmania* DUBs through the complex life cycle of the parasite. Our bioinformatic analysis identified 20 DUBs belonging to the C12, C19 and C65 peptidase families, suggesting an extensive deubiquitinating system in *L. mexicana*, comparable in size to *Saccharomyces cerevisiae* [35]. Additional cysteine peptidase DUBs from C78, C85 and clan CP C97 families have been characterised in another study [26]. Analysis of DUBs in promastigote lysates using the Cy5UbPRG ABP probe identified 6 active DUBs (DUB2, DUB15, DUB16, DUB17, DUB18 and DUB19) by mass spectrometry and additional active enzymes by in-gel fluorescence, demonstrating the presence of an active deubiquitinating system in *L. mexicana*. Additional active DUBs were identified by in-gel fluorescence comparison of wild type and gene deletion mutants (DUB6, DUB9), yet many remain unidentified and could be active below the limit of

detection or possibly expressed in life cycle stages in the sandfly that were not examined in this study. We also used the ABP to demonstrate that many of the DUBs have activity that appears to remain constant in the different life cycle stages, yet we also demonstrated that Δ*dub4*, Δ*dub7* and Δ*dub13* had no detectable loss of fitness in the promastigote, but had a significant loss of fitness in the amastigote. This apparent contradiction might be explained by a specific requirement for stage-regulated DUB substrates. Intracellular amastigotes have a stringent metabolic response that is acutely sensitive to metabolic perturbation [36]. Our data indicate that amastigotes are also highly sensitive to disruption of ubiquitination homeostasis.

The bar-seq screen and individual viability assay of DUB null mutants highlighted DUBs with potential roles in differentiation and infection. Δ*dub4*, Δ*dub7* and Δ*dub13* had the strongest loss of fitness defects observed in axenic amastigote, macrophage infection and mouse infection experiments. Additionally, Δ*dub3*, Δ*dub5*, Δ*dub6*, Δ*dub8*, Δ*dub10*, Δ*dub11* and Δ*dub14* showed strong loss of fitness uniquely during mouse infection, perhaps due to increased selective pressures inside the host or the longer duration of the experiment. Although we identified a number of life cycle defects using the bar-seq screen, there are some potential limitations to using a pooled library, as the fitness of individual null mutants may be influenced by other mutants in the pool. This may explain, for example, the different phenotypes observed for Δ*dub9* between the bar-seq experiment and viability assay/HASPB blot. Our individual profiling of axenic amastigote null mutants using the viability assay confirms the phenotypes we observed in the bar-seq screen, but further individual assessment on selected null mutant lines could be advantageous. The identification of several DUBs essential for differentiation was not unexpected as the *Leishmania* proteome differs substantially between promastigote and amastigote stages [37]. DUBs can control the abundance of *Leishmania* proteins by rescuing them from proteasomal degradation or, more indirectly, by regulating autophagy. Autophagy has been shown to be essential for the differentiation of promastigotes into amastigotes both *in vitro* and *in vivo* [33, 38]. Proteolysis is required for metacyclogenesis and the promastigote to amastigote transition [39] and an accumulation of ubiquitylated proteins in the cytosol has been documented at the onset of differentiation [40]. Therefore, a role for *Leishmania* DUBs in differentiation-associated protein degradation could explain the higher degree of essentiality observed for DUBs over other peptidases in our bar-seq screen.

We were unable to generate null mutant lines for four DUBs, three C19 (DUB1, DUB2 and DUB12) and one C12 family (DUB16) peptidase. The successful generation of facilitated null mutant lines for the four DUBs provides a level of support that they are essential for the promastigote. DUB16 is related to human UCHL1 (33% identity) and UCHL3 (37% identity), for which one proposed role is the control of free ubiquitin levels through the processing of ubiquitin precursor and ubiquitinated proteins [41]. DUB16 could have a role in regulating free ubiquitin levels, something that must be further investigated.

USP36 is the human DUB most closely related to DUB12 (28% identity) and has been shown to regulate the stability of nuclear proteins including c-Myc, B23 and fibrillarin, the latter two of which are required for rRNA processing and ribosomal biogenesis [42]. USP36 deletion is lethal in mice, attributable to its role in rRNA processing and protein synthesis [43]. However, deletion of the yeast homologue, Ubp10, only results in a reduced growth phenotype [44]. Further investigation must be performed to investigate if DUB12 shares any functional similarity with USP36 and to explain how DUB12 depletion caused cell death. Lastly, for the DUB12 overexpression line, we observed an increase in the activity of two forms of DUB12, likely arising from its proteolytic cleavage to 55 kDa proteins from an 85 kDa precursor. The post-translational modification of DUBs is one way in which their activity has been shown to

be regulated and, although rare, proteolytic cleavage of DUBs has been described for some human DUBs [45, 46].

DUB2 is a cysteine peptidase with a C19-UCH domain, a UBA domain at the C-terminus and a ZnF_UBP domain at the N-terminus. The most similar human DUBs are USP5 and USP13. USP5 is a well characterised member of the USP family responsible for the disassembly of the majority of unanchored poly-ubiquitin *in vivo* [47]. The ZnF-UBP domain of USP5 recognises the C-terminus of ubiquitin [48] and USP5 has been shown to hydrolyse Lys-63, Lys-48, Lys-11, Lys-29 linkages [49]. DUB2 is similar to USP5 in having broad linkage specificity towards all the di-ubiquitin chains except Met-1 and Lys-29 *in vitro*. Our *in vitro* experiments demonstrate that DUB2 exhibits deubiquitinating activity against both artificial DUB substrates (Cy5-Ub-PRG ABP and Ub-AMC) and di-ubiquitin. Several human DUBs have previously been demonstrated to have a pleiotropic function by regulating protein stability or by regulating assembly and function of different machineries. Similarly, the essentiality, localisation and interactome of DUB2 suggests a pleiotropic role in the deubiquitination of multiple substrates. The possibility that DUB2 is responsible for the release of ubiquitin from polyubiquitin chains could also explain the phenotype in *Leishmania* after DUB2 depletion. The sudden and significant depletion of free ubiquitin results in significant dysfunction of all molecular machinery associated with ubiquitin, such as proteasomal degradation, endocytosis, replication, transcription and RNA splicing. If this was the case, the parasite would enter a 'free ubiquitin crisis', which would eventually lead to death.

The interactome data suggest DUB2 plays a role in post-transcriptional gene regulation. In *Leishmania* and other kinetoplastids, gene expression occurs in an unusual manner involving constitutive polycistronic transcription and *trans*-splicing of a splice leader RNA to generate mature mRNAs [50]. Amongst the DUB2 interactors, one of the most strongly enriched proteins was cyclin 12 which in trypanosomes forms a tripartite complex with CRK9 and a CRK9-associated protein, CRK9AP. The CYC12-CRK9-CRK9AP complex is essential for *trans*-splicing of the splice leader RNA [30]. However, CRK9 and CRK9AP were not detected in the DUB2 interactome, indicating that DUB2 may play a role in turnover of free CYC12. Depletion of CRK9AP causes a rapid loss of CYC12 at the protein but not mRNA level, suggesting dynamic regulation of CYC12 protein [30]. DUB2 may therefore protect free CYC12 from degradation. When DUB2 is absent, CYC12 may become a target for degradation, leading to co-depletion of CRK9 and a critical loss of *trans* splicing capacity. Alternatively, deubiquitination of CYC12 may be required for complex formation, similar to the requirement for the removal of ubiquitin from Bcl10 by Usp9x for its tripartite complexing to Malt1 and Carma1 [51]. Another strongly enriched protein in the DUB2 interactome was the histone chaperone NAP1, an important factor in nucleosome assembly [31]. This implies a role for DUB2 in nucleosome dynamics. In other eukaryotes, ubiquitination/de-ubiquitination of H2A and H2B is a dynamic process that modulates the stability of nucleosomes to allow transcription/DNA replication to take place [52]. The transcription factors, splicing factors and DNA replication proteins co-enriched with DUB2 are consistent with a role in regulating nucleosome assembly/disassembly since this would place DUB2 in the vicinity of these processes.

DUB activity can be regulated by post-translational modifications such as phosphorylation, for which one of the best characterised examples is activation of OTUD5/DUBA (OTU-domain-containing protein 5) by phosphorylation in the catalytic domain [53]. Ubiquitination can also affect DUB activity, for example, ubiquitination of UCH-L1 near the active site prevents binding to ubiquitin [54]. We identified a phosphorylated region and a ubiquitination site flanking the DUB2 UBA domain which could similarly regulate binding of DUB2 to ubiquitinated substrates. DUB2 has a broad specificity for diubiquitin cleavage, with Lys-27 being

the only linkage for which there is poor activity. Lys-11, Lys-29 and Lys-48 linked chains have roles in proteasomal degradation, Lys-29 is associated with lysosomal degradation and Lys-33 is involved in both secretory and endocytic pathways, acting as a sorting signal for membrane proteins [55]. Another preferred linkage of DUB2 is Lys-63 which can serve as a molecular glue, allowing the rapid and reversible formation of pivotal signalling complexes. Lys-63 ubiquitin chains have been shown to regulate several biological processes including DNA repair, clearance of damaged mitochondria and protein sorting and they can guide assembly of large protein complexes that drive mRNA splicing and translation [55]. In the DUB2 pull down, the VPS4 protein was identified, which could indicate a putative role of DUB2 in endosome sorting and could explain why DUB2 cleaves Lys-33 and Lys-29. Whilst VPS4 is the only known protein associated with autophagy/endocytosis that was identified in the DUB2 interactome, a role in the endocytic system fits with DUB2 lysosomal localisation. Previously, VPS4 was shown to play a role in endosome sorting and autophagy in *L. major*, which are essential for the differentiation and virulence of this parasite [33].

In the past decade there has been an expanding interest in DUBs as potential drug targets as they have been shown to play a crucial role in both cancer and neurodegenerative diseases [56]. The determination of the structure of multiple DUBs, including catalytic domains, in combination with the development of advanced high-throughput screening-compatible assays with USP substrates has resulted in the discovery of several inhibitors against a select number of human DUBs including USP7 [57, 58] and USP14 [59]. *DUB2* is the first DUB to have been genetically validated as a drug target in *L. mexicana*. DiCre permitted the analysis of emerging phenotypes, confirming the essential role for DUB2 in promastigotes and in the establishment of mouse infection. Analysing *Leishmania* genes in this manner represents a high level of genetic validation [60]. To date, most drug target validation has relied on genetic manipulation of promastigotes, however, the bar-seq approach presented here has revealed some DUBs to have amastigote-specific loss of fitness, making DUBs 3, 5, 6, 8, 10, 11 and 14 potential drug targets. As DUB6 is related to human USP7 and DUB14 to human USP14, chemical tools developed for human DUB drug discovery programs [59] may be useful chemical entry points to develop inhibitors to the *Leishmania* enzymes.

Materials and methods

Ethics statement

All experiments were conducted according to the Animals (Scientific Procedures) Act of 1986, United Kingdom, and had approval from the University of York Animal Welfare and Ethical Review Body (AWERB) committee.

Culture of *Leishmania*

Leishmania mexicana (MNYC/BZ/62/M379) were grown in HOMEM (Gibco) supplemented with 10% (v/v) heat-inactivated foetal calf serum (HIFCS) (Gibco) and 1% (v/v) Penicillin/ Streptomycin solution (Sigma-Aldrich) at 25˚C. Mid-log phase parasites were defined as between $4–8 \times 10^6$ cells mL^{-1} and stationary phase parasites between $1.5–2.5 \times 10^7$ cells mL^{-1}.

L. mexicana promastigotes were differentiated to axenic amastigotes as previously described [61]. Briefly, stationary phase culture of *L. mexicana* was pelleted by centrifugation at 1,000 x g for 10 minutes and washed with 1 x PBS. Cells were then resuspended in amastigote culture medium (Schneider's Drosophila medium [Gibco], 20% HIFCS and 0.015 mg mL^{-1} hemin [stock dissolved in 50 mM NaOH], pH 5.5) with a concentration of 2×10^6 cells mL^{-1} in 6-well plates. Except where stated otherwise, cells were then incubated at 32˚C with 5% CO_2. For transformation of amastigotes back to promastigotes after 120 h, 100 μL of axenic amastigotes

were diluted in 5 mL of HOMEM medium with 10% HIFCS and 1% Penicillin/Streptomycin and placed in 6-well plates. The plate was then incubated at 25˚C. Transgenic parasites were grown with the following antibiotic concentrations: G418 (Neomycin) at 50 μg mL^{-1}; Hygromycin at 50 μg mL^{-1}; Blasticidin S at 10 μg mL^{-1}; Puromycin at 30 μg mL^{-1} (antibiotics from InvivoGen). To assess viability assay of axenic amastigotes, 200 μL of axenic amastigotes at 1 x 10^6 cells mL^{-1} were placed in 96 well plates and incubated at 35˚C with 5% CO$_2$. 20 μL of 0.05 μM resazurin (Sigma) was added and the plate was incubated overnight as before. The next day, resorufin fluorescence (579 Ex/584 Em) was measured using a Polarstar plate reader (Omega).

To assess infection of mice, 10^6 stationary phase *L. mexicana* promastigotes were injected into the right footpad of female BALB/c mice (Charles River Laboratories). Lesion size was monitored weekly. Parasite burden was assessed as previously described [62]. For profiling of DUBs in lesion-derived amastigotes, 4 x 10^6 stationary phase *L. mexicana* were injected into the rump of female BALB/c mice. Lesion size was monitored weekly. For the purification of lesion derived amastigotes the lesion tissue was collected in amastigote stabilisation buffer (PSGEMKA) [63], cut into pieces and passed through a sterile 100 μm cell strainer (BD) to disrupt the host macrophages and liberate the amastigotes. The suspension was incubated with 125 mg L^{-1} saponin for 5 mins, centrifuged 2,000 x g for 10 mins and the pellet was washed twice with PSGEMKA buffer. Cell debris was eliminated by passage through a glass wool— Sephadex CM-25 column. The suspension obtained was centrifuged at 2,000 x g for 10 mins. Thereafter, the supernatants were discarded, and the pellets were resuspended in Schneider's Drosophila medium supplemented as indicated above.

L. mexicana transfections were performed using a T Cell Nucleofector Kit (Lonza) as described previously [26]. The transfected culture was split between two flasks to select for independent transfection events and incubated overnight at 25˚C to recover. The next day, suitable antibiotics were added and cells cloned by serial dilutions of 1 in 6, 1 in 66 and 1 in 726 in 96-well microplates.

Phylogenetic analysis

The protein sequences for DUBs were extracted from (Uniprot- https://www.uniprot.org/) [64]. For human DUBs the canonical sequence was used as it was determined by Uniprot. The protein alignment was performed using MUSCLE (multiple sequence alignment with high accuracy and high throughput). A constraint tree was created by including DUBs into the seven known families and a phylogenetic tree was generated by RAxML (https://raxml-ng. vital-it.ch/#/) [65]. The LG Substitution matrix was used. The best fit model tree was further designed initially in the iTOL INTERACTIVE TREE OF LIFE (https://itol.embl.de/) where branch length was ignored, and an unrooted tree style was formed. Finally, Adobe Illustrator was then used to finalise the tree.

Life cycle phenotyping using bar-seq

Null mutants were generated using a CRISPR-Cas9-based approach [23] with a cell line expressing Cas9 and T7 RNA polymerase [26]. DNA was harvested from clones or populations for diagnostic PCRs using the QIAGEN DNeasy Blood and Tissue Kit. Two sets of primers were designed to confirm the generation of null mutants, the first specific to the ORF of the target gene and the second specific to the UTRs (forward primer 5'-UTR, reverse primer 3'-UTR).

Null mutant lines were grown to mid-log phase, spun down at 1,000 x g for 10 min and pooled in equal proportions in Grace's medium (Grace's insect media [Sigma-Aldrich] with

4.2 mM NaHCO$_3$, 10% FCS [Gibco], 1 x Penicillin/Streptomycin [Gibco] and 1 x BME Vitamins [Sigma-Aldrich] and adjusted to pH 5.25) up to a total concentration of 2 x 10^6 cells mL^{-1}. Cultures were prepared in sextuplicate to provide technical replication. Next, the pooled cells were grown at 25˚C for 7 d to allow for the enrichment of metacyclic promastigotes. To prepare axenic amastigotes, promastigotes from the 168 h time point were centrifuged and resuspended in amastigote medium at 2 x 10^6 cells per well. Cells were then cultured at 35˚C with 5% CO$_2$.

Bone marrow-derived macrophages were extracted from female BALB/C mouse femur, equilibrated in warm DMEM (GE Life Sciences), spun at 200 x g for 10 min and resuspended in macrophage medium (DMEM [Invitrogen] plus 10% FCS and 2 mM L-glutamine) in order to have 2.5 x 10^6 cells per well [66]. Enriched metacyclic cells were purified using a Ficoll 400 (Sigma-Aldrich) gradient (40%, 10% and 5% Ficoll) and centrifuged at 1,300 x g for 10 min. Following washing with Grace's medium, metacyclic promastigotes were added to the macrophages in a 1:1 ratio and left to interact for 4 h at 35˚C with 5% CO$_2$. Excess *Leishmania* cells were then removed by washing with DMEM and the cells incubated in DMEM 10% HIFCS for 12 h and 72 h.

To perform the mouse infections, 10^6 purified metacyclic promastigotes were injected into the left footpad of BALB/c mice. Mice were culled at 3 and 6 weeks post-inoculation. At the relevant time points, DNA was extracted from experimental samples and processed using the QIAGEN DNeasy Blood and Tissue Kit. DNA samples were prepared for next-generation sequencing by first amplifying unique barcodes by PCR using the following primers: 5'-TCG TCGGCAGCGTCAGATGTGTATAAGAGACAGAgatgatgattacTAATACGACTCACTA TAAAACTGGAAG-3' and 5'-GTCTCGTGGGCTCGGAGATGTGTATAAGAGACAGGA GAGACAGGCATGCCTT-3' containing the Illumina adapter sequence. Reactions were set up with Q5 polymerase (NEB) as per the manufacturer's instructions except for the following changes: just 0.5 x of Q5 Reaction Buffer and Q5 High GC Enhancer were used. The cycling conditions were 98˚C for 5 min followed by 20–25 cycles of 98˚C for 30 sec, 60˚C for 30 sec and 72˚C for 10 sec. Following purification of the PCR reactions using the QIAGEN MinElute PCR Purification Kit, a second PCR was performed using Illumina's Nextera XT indexing primers in order to add unique barcode sequences to each sample. 8 cycles of PCR amplification were performed using NEBNext Q5 Polymerase 2X Master Mix (New England Biolabs), according to the manufacturer's guidelines. Indexed amplicons were purified using 0.9 X AMPure XP beads (Beckmann Coulter) and eluted into low TE buffer before quantitation and pooling at approximately equimolar ratios. Amplicon pools were then sent for 150 base paired end sequencing on an Illumina HiSeq 3000 sequencer at the University of Leeds Next Generation Sequencing Facility.

Illumina read sequences were analysed using a custom Python script to search for the 12 bp sequence preceding the barcode. If an exact match was found, the following 12 bp sequence was counted as a barcode sequence. A total count for each unique barcode sequence was generated for each sample. Next, the relative fitness of null mutants at each life cycle stage was calculated by taking the number of unique barcode reads for each null mutant line and dividing it by the total number of expected barcode reads. Significant increases or decreases in null mutant line fitness between adjacent samples in the experimental workflow were analysed using unpaired t-tests and the Holm- Šídák method in GraphPad Prism 7.

Construction of plasmids

A full list and descriptions of all primers and plasmids used in this study can be found in S3 Table. The construction of the plasmids needed for the generation of *DUB2* inducible gene

deletion was performed as previously described [29]. The *DUB2* gene including stop codon was cloned into pGL2315, creating pGL2727. For the complementation plasmids, pNUS-*DUB1*, *DUB2*, *DUB12 and DUB16* expression plasmids were generated using Gibson Assembly. The successful clones were confirmed using PCR and sequencing.

Induction of diCre mediated gene deletion

A modified version of the DiCre inducible system [29] was used. Two dimerisable Cre recombinase subunits were integrated into the ribosomal locus. DiCre in cell lines containing both diCre and loxP flanked genes of interest was induced by the addition of between 100 nM and 1 μM rapamycin (Abcam). Promastigotes were then allowed to grow for 48 h and split into new cultures with a concentration of 1×10^5 cells mL^{-1} and induced again with 100 nM of rapamycin.

Viability analyses

2–5×10^6 *L. mexicana* promastigotes were pelleted by centrifugation at 1,000 x g for 10 mins and washed twice with PBS with 5mM of EDTA. Cells were resuspended in 1mL of PBS with 5mM EDTA and 1μg mL^{-1} of propidium iodide (PI) and 1 μg mL^{-1} of RNAse A. Cell fluorescence was analysed on a Beckman Coulter, CyAn ADP. Data were analysed on FlowJo software (Tree Star Inc.).

Preparation of protein extracts

3×10^7 *L. mexicana* cells in the desired life cycle stage were pelleted by centrifugation at 1,000 g for 10 min. Cells were washed in 1 x PBS and lysed by resuspending in 40 μL of 1 x SDS-PAGE loading buffer. Next, samples were heated for 10 minutes at 90°C on a heat block. Samples were allowed to cool down at room temperature and 250 U of Expedeon BaseMuncher endonuclease was added to each sample. Samples were then incubated at 37°C for 30 minutes and loaded directly into a NuPAGE 4–12% Bis-Tris protein gel (Thermofisher) or stored at -20°C.

Cy5UbPRG profiling

3×10^7 cells from a log-phase *L. mexicana* culture or 9×10^7 amastigote were spun at 1,000 x g and washed three times with 1 mL of ice-cold TSB Wash buffer (44 mM NaCl, 5 mM KCl, 3 mM NaH$_2$PO$_4$, 118 mM sucrose and 10 mM glucose, pH 7.4). Next, the cells were lysed using a newly prepared ice-cold lysis buffer (50 mM Tris-HCl pH 7.4, 120 mM NaCl, 1% NP40 and freshly added in order: 1 μg mL^{-1} pepstatin, 1 x cOmplete ULTRA Tablets, [Mini, EASYpack Protease Inhibitor Cocktail, Roche], 1 mM DTT, 1 mM PMSF, 0.01 mM E64). Samples were incubated at 4°C for 15 minutes. Afterwards, samples were centrifuged at 17,000 x g for 15 minutes and the supernatant withdrawn. Samples were prepared to have a protein concentration of 1 mg mL^{-1} in a total volume of 25 μL. 2 μL of 50 mM NaOH and 1 μM of Cy5UbPRG (UbiQ) were added. Lysis buffer was used to top up to a final volume of 25 μL. The reaction was then incubated at room temperature for 30 min and stopped by the addition of 3 x loading dye. 12 μL were then analysed in a gradient 4–12% NuPage Bis-Tris protein gel, for exactly 90 min at 200 V. The gel was then washed with water and imaged with Amersham Typhoon with Excitation: 635 nm, Filter: Cy5 670BP30 (GE Healthcare Life Sciences).

For purification of DUBs cyanogen bromide (CNBr)-activated Sepharose 4B resin (GE Healthcare) was used to couple with Ub-PRG (1.2 pmol) or Ubiquitin (1.2 pmol) according to the manufacturer's protocol (GE Healthcare). Beads were then stored in 4°C until used. 50 mg of the coupled resin of either Ub-PRG or ubiquitin were incubated with fresh *Leishmania*

lysate collected from 1 x10^8 cells (prepared as described above) at 37˚C for 3 h. The beads were then washed with PBS plus 1% Triton X-100 (3 x 10 mL), 2% CHAPS, 8 M Urea in PBS and distilled water. The bound proteins were then digested on-bead with trypsin and analysed by MS/MS spectrometry. The MS data was processed using Data Analysis software (Bruker) and the automated Matrix Science Mascot Daemon server (v2.4.1). Protein identifications were assigned using the Mascot search engine to interrogate protein sequences in the annotated proteins database (obtained from TriTrypDB), allowing a mass tolerance of 0.4 Da for both MS and MS/MS analyses.

Immunoprecipitation of myc-tagged *Leishmania* proteins

For each of a total of 3 independent replicates, 1 x 10^9 parasites were washed twice in PBS and cross-linked with 1 mM dithiobis(succinimidyl propionate) (DSP, Thermo Scientific) in 10 ml PBS for 10 min at 26˚C. DSP was quenched with 20 mM Tris pH 7.5 for 5 min. Parasites were lysed in ice cold 500 µl lysis buffer (1% NP40, 50 mM Tris pH 7.5, 250 mM NaCl, 1 mM EDTA, 0.1 mM PMSF, 1 µg mL^{-1} pepstatin A, 1 µM E64, 0.4 mM 1–10 phenanthroline, 20 µl mL^{-1} proteoloc (Expedeon), 0.17 complete protease inhibitor tablets mL^{-1} (Sigma)) by probe sonication for 3 × 5 sec. Lysate was centrifuged for 10 min at 10,000 x g at 4˚C and protein concentration in the supernatant measured by BCA assay (Thermo scientific). Lysate equivalent to 5 mg of total protein was incubated with 30 µl anti-myc magnetic beads (Thermo scientific) for 2.5 hr at 4˚C with rotation. Beads were washed 4 × 300 µl ice cold lysis buffer for 5 min each wash followed by two PBS washes. Beads were then stored at -80˚C. Myc-tagged protein was eluted at room temperature with 25 µl myc-peptide (0.5 mgmL^{-1} in PBS, Sigma) for 15 minutes at 700 rpm mixing. The elution step was repeated and eluates pooled. 1/10th of the elution was used to check successful immunoprecipitation by western blot. The remainder was mixed with 4 volumes of absolute methanol and 1 volume of chloroform and vortexed for 1 min. The sample was then centrifuged for 1 h at 18,000 x g at 4˚C. The pellet was washed with 270 µL of absolute methanol and centrifuged for 10 min at 18,000 x g at room temperature. The pellet was resuspended in 150 µL 50 mM TEAB pH 8.5, 0.1% PPS silent surfactant (Expedeon) for 1 h by shaking at 800 rpm at room temperature. Afterwards, 10 mM of Tris (2-carboxyethyl) phosphine (TCEP) and 10 mM Iodoacetamide (IAA) were added to the sample and incubated for 30 min at room temperature in the dark. Finally, 200 ng of trypsin and 1 mM CaCl$_2$ were added and proteins digested overnight at 37˚C 200 rpm. After digestion, PPS silent surfactant was cleaved by acidifying the digest to 0.5% trifluoroacetic acid (TFA) and incubating 1 h at RT. Digest was centrifuged for 10 min at 17,000 x g. Peptides were desalted with C18 (3M Empore) desalting tips.

Samples were loaded onto an UltiMate 3000 RSLCnano HPLC system (Thermo) equipped with a PepMap 100 Å C18, 5 µm trap column (300 µm x 5 mm Thermo) and a PepMap, 2 µm, 100 Å, C18 EasyNano nanocapillary column (75 µm x 150 mm, Thermo). The trap wash solvent was aqueous 0.05% (v:v) trifluoroacetic acid and the trapping flow rate was 15 µL min^{-1}. The trap was washed for 3 min before switching flow to the capillary column. Separation used gradient elution of two solvents: solvent A, aqueous 1% (v:v) formic acid; solvent B, aqueous 80% (v: v) acetonitrile containing 1% (v:v) formic acid. The flow rate for the capillary column was 300 nL min^{-1} and the column temperature was 40˚C. The linear multi-step gradient profile was: 3–10% B over 7 min, 10–35% B over 30 min, 35–99% B over 5 min and then proceeding to wash with 99% solvent B for 4 min. The column was returned to initial conditions and re-equilibrated for 15 min before subsequent injections. Each independent replicate was injected once.

The nanoLC system was interfaced with an Orbitrap Fusion Tribrid mass spectrometer (Thermo) with an EasyNano ionisation source (Thermo). Positive ESI-MS and MS2 spectra

were acquired using Xcalibur software (version 4.0, Thermo). Instrument source settings were: ion spray voltage, 1,900 V; sweep gas, 0 Arb; ion transfer tube temperature, 275˚C. MS1 spectra were acquired in the Orbitrap with: 120,000 resolution, scan range: m/z 375–1,500; AGC target, 4e5; max fill time, 100 ms. Data dependent acquisition was performed in top speed mode using a 1 sec cycle, selecting the most intense precursors with charge states >1. Easy-IC was used for internal calibration. Dynamic exclusion was performed for 50 sec post precursor selection and a minimum threshold for fragmentation was set at 5e3. MS2 spectra were acquired in the linear ion trap with: scan rate, turbo; quadrupole isolation, 1.6 m/z; activation type, HCD; activation energy, 32%; AGC target, 5e3; first mass, 110 m/z; max fill time, 100 msec. Acquisitions were arranged by Xcalibur to inject ions for all available parallelisable time.

Peak lists in.raw format were imported into Progenesis QI (Version 2.2., Waters) and LC-MS chromatograms aligned. Precursor ion intensities were normalised against total intensity for each acquisition. A combined peak list was exported in.mgf format for database searching against the *L. mexicana* subset of the TriTrypDB database (8,250 sequences; 5,180,224 residues). Mascot Daemon (version 2.6.1, Matrix Science) was used to submit the search to a locally-running copy of the Mascot program (Matrix Science Ltd., version 2.6.1). Search criteria specified: Enzyme, trypsin; Max missed cleavages, 2; Fixed modifications, Carbamido-methyl (C); Variable modifications, Oxidation (M), Phosphorylation (S,T,Y); Peptide tolerance, 3 ppm; MS/MS tolerance, 0.5 Da; Instrument, ESI-TRAP. Peptide identifications were passed through the percolator algorithm to achieve a 1% false discovery rate as assessed against a reversed database and individual matches further filtered to minimum expect scores of 0.05. The Mascot.XML result file was imported into Progenesis QI and peptide identifications associated with precursor peak areas. Relative protein abundance was calculated using precursor ion areas from non-conflicting unique peptides. Accepted protein quantifications were required to contain a minimum of two unique peptide matches. Interactors were scored using SAINTq [67], using a false discovery rate threshold of <1% to select high confidence DUB2 interactors. Complete mass spectrometry data sets are available to download from MassIVE (MSV000085242) and ProteomeXchange (PXD018415). The doi for the data is [doi:10.25345/C5Z10J].

Protein expression and purification

A baculovirus expression system was used for the expression of DUB2 recombinant protein in sf9 insect cells as described in the Bac-to-Bac Baculovirus Expression protocol (Invitrogen). The gene was first cloned into the PFastBacNKI-his-3C-LIC vector using Ligation Independent Cloning (LIC). After three days, the insect cells were lysed in lysis buffer (30 mM Tris-HCl, pH 8, 0.3 M NaCl, 0.03 M imidazole, 5 mM β-mercaptoethanol and 1 tablet of cOmplete ULTRA Tablets, Mini, EASYpack Protease Inhibitor Cocktail, Roche) by sonication. The samples were then centrifuged (21 K, 4˚C, 30 min) and the supernatant applied to an AKTA Start (GE Life Sciences) at 5 mL min^{-1}, to a 5 mL His- trap crude FF column (GE Life Sciences). This was washed with Buffer A (30 mM Tris-HCl pH 8, 0.3 M NaCl, 0.03 M imidazole, 5 mM β-mercaptoethanol) and the protein eluted with increasing concentration of imidazole (0.03–0.5 M). Protein was concentrated using Amicon Ultra-4 30k MWCO (Millipore). 3C protease was added to purified protein in a 1:50 (w:w, 3C:Recombinant protein) ratio with 2 mM DTT. The aliquot was added to a 16 kDa dialysis tube and incubated at 4˚C in buffer A overnight. Protein was loaded onto a 5 mL His-trap crude FF column and ran as described above. The flow-through from the His-tag cleavage containing the tag free protein was concentrated to 2 mL using Amicon Ultra-4 30k MWCO (Millipore). The concentrated protein was applied to a HiLoad 16/600 S75pg column (GE Life Sciences), equilibrated and eluted in 25 mM Tris-HCl

pH 8.0, 150 mM NaCl, 5 mM β-mercaptoethanol. Fractions containing the protein were identified by absorbance at 280 nm and analysed by 10% SDS-PAGE. These fractions were pooled and concentrated up to 2 mg mL^{-1}. 1 mM of DTT was added to the sample and the protein stored at -80˚C.

Ubiquitin probe assay for recombinant protein

10 μL of the appropriate concentration of the recombinant DUB was incubated with 2 μL 50 mM NaOH, 5 μL dH$_2$O and 2 μL 0.25 μg mL^{-1} ubiquitin probe Cy5UbPRG (UbiQ) for 30 min at room temperature. Binding of probe was analysed using a NUPAGE 4–12% Bis-Tris Gel. The gel was then scanned using the Amersham Typhoon (GE Healthcare Life Sciences) and stained with InstantBlue Protein Stain.

The in *vitro* enzymatic assay with the fluorogenic substrate ubiquitin-7-amido-4- methyl-coumarin (Ub-AMC, UbiQ) was assembled in a 384-well microplate (Thermo Scientific). Assays were performed in 20 μL reaction volumes and in triplicate. The reactions were initiated by the addition of 10 μL of substrate or enzyme. Substrate and enzymes were diluted in buffer containing 50 nM Tris, pH 8.0, 0.15 M NaCl, 5 nM DTT and 0.05% CHAPS. The fluorescence intensity was monitored with a Polarstar plate reader (Omega) equilibrated at 25˚C at intervals of 20 sec for 20 min using excitation/emission filter pairs of 340/460 nm. The fluorescence value was then converted into concentration using a standard curve. The standard curve was determined by allowing the reactions to plateau and the maximum arbitrary fluorescence units were measured and plotted against a known substrate concentration. An AMC concentration against time graph was generated in Excel software and the initial slope of each reaction was determined by generating a linear regression. For the determination of the Km and kcat values of DUB2, the enzyme concentrations were kept constant, and the concentration of Ub-AMC varied from 0.25 μM to 32 μM. The initial rates in μM sec^{-1} were then plotted against substrate concentration (μM) in Prism 7 software. The data were fitted to the Michaelis-Menton equation so the kinetic parameters, Km and kcat were determined.

Supporting information

S1 Fig. Protein sequence alignment of *Leishmania* DUBs. Multiple protein sequence alignment of *Leishmania* DUBs and selected reference human DUB sequences showing their active residues. Human DUB sequences were obtained from UniProtKB: PAN2 (Q504Q3), USP7 (Q93009), USP8 (P40818), BAP1 (Q92560), UCHL1 (P09936), UCHL3 (P15374), UCHL5 (Q9Y5K5), OTUB1 (Q96FW1), OTUB2 (Q96DC9) and OTULIN (Q96BN8). C19, C12 and C65 DUB families were aligned using the T-Coffee multiple sequence alignment program. A yellow star represents the active cysteine and the blue star represents the active histidine. (TIF)

S2 Fig. Generation of the DUB null mutant library. Diagnostic PCRs were performed to check the successful generation of null and facilitated null mutants. PCR analysis of genomic DNA of at least two individual clones (null mutants, CL1, CL2 etc) or two separate populations (facilitated null mutants), using the indicated set of primers: ORF-specific primers (A), UTR-specific primers (B) or ORF-specific, 5'-UTR-blasticidin or UTR-specific primers (C). As a control, the parental Cas9 T7 cell line was used. The resulting amplicons were resolved on a 1% agarose gel and stained with SYBR safe. The expected size of the resulting amplicons is presented in S3 Table. A schematic representation of the wild type, heterozygous, null mutant and facilitated null mutant genomic loci including the diagnostic primers (green arrow primers bind to ORF, grey arrow primers bind to UTRs and amplify across the loci, purple arrow

primers binds to the blasticidin resistance marker) is also shown in (C).
(TIF)

S3 Fig. Activity profiling of the DUB null mutant cell lines. (A) Lysate extracted from log-phase *L. mexicana* promastigotes treated with or without Cy5UbPRG for 30 min. Proteins were separated by SDS-PAGE and in-gel fluorescence (Cy5) was captured using a Typhoon imager followed by Coomassie staining as a loading control. (B) Lysates extracted from null mutant lines of log-phase *L. mexicana* promastigotes treated with Cy5UbPRG for 30 min. In-gel fluorescence images were obtained as for (A). The red arrowhead shows the position where an active DUB is missing compared to the parental Cas9 T7 cell line. (C) Western blot analysis of 2×10^7 axenic amastigotes. Samples were separated in a 4–15% protein gel. The stain-free gel used contains trihalo compounds which, in the presence of the UV-light, react with trypto-phan residues, producing fluorescence. The gel was activated by 45 sec UV exposure, proteins were transferred to a PVDF membrane and probed with 1:1,500 dilution of anti-HASPB. Finally, as a loading control the total protein was determined using the stain-free property of the gel. (D) Lysate extracted from differentiated promastigotes to axenic amastigotes (48 h and 144 h after initiation of axenic differentiation) treated with or without Cy5UbPRG for 30 min. Protein was separated in an SDS-PAGE gel, and the image was captured using a Typhoon imager and the gel stained with Coomassie.
(TIF)

S4 Fig. Localisation of endogenously tagged DUB2. Live cell imaging of *L. mexicana* procyclic promastigotes expressing mNeonGreen (mNG) tagged DUB2. DNA is stained with Hoechst 33342 and a representative selection of images is shown. DIC, differential interference contrast.
(TIF)

S5 Fig. Generation and validation of *DUB2* inducible cell line. (A) Left: PCR analysis of extracted gDNA demonstrates successful integration of *HYG* cassette. The replacement of *DUB2* wild type allele with the *HYG* cassette was detected by PCR amplification using the primers shown in the schematic (right). The forward primer was designed to bind to the ORF of *DUB2* whereas the reverse primer binds on the 3' UTR of the target gene. Black arrows represent the primers. (B) PCR amplification of *DUB2*$^{-/+FLOX}$ Clone 4, 6, *DUB2*$^{-/+FLOX}$ [*DUB2*] and *DUB2*$^{-/+FLOX}$ [*DUB2*^{C312A}] surviving parasites after treatment with RAP in the clonal assay (Fig 4E). Schematic representation of the primers used for the PCR as well as the expected fragments are shown in Fig 4A. (C) Compiled flow cytometry results of live/dead cells detected using propidium iodide staining in *DUB2*$^{+/+flox}$ and *DUB2*$^{-/+flox}$ promastigotes over the course of 96 hours post induction. Cells were grown for 48 hours with or without rapamycin. Afterwards, the cells were seeded at a density of 1×10^5 cells mL^{-1} and allowed to grow in the presence or absence of 100 nM of RAP. Samples were collected every 24 h. Flow cytometry was used to analyse the samples. The data were then collected and analysed with FlowJo_v10 software, where the percentage of dead cells was determined. The data were analysed in Prism software and an unpaired t-test performed to indicate significance (n = 3) between different time points, comparing treated with RAP to untreated samples. Error bars indicate the standard deviation of a mean. ***p $<$ 0.001, ****p $<$ 0.0001.
(TIF)

S6 Fig. DUB2 Immunoprecipitation using anti-myc beads. (A) DUB profiling using the ABP Cy5UbPRG. Cell extract from a WT and mNeon:DUB2 was incubated with Cy5UbPRG for 30 min. Proteins were then separated by SDS-PAGE and imaged. The yellow arrow represents the DUB2 WT band whereas the red arrow represents the mNeon-DUB2. (B) Western

blotting analysis with anti-myc antibody (1:2,000) of protein cell extract from samples collected after immunoprecipitation of control cell line (WT) and mNeon:DUB2. E1, E2 were samples collected from the elution (myc peptide 0.5 mg mL^{-1} in PBS).
(TIF)

S7 Fig. Purification of DUB2 active (left) and DUB2^{C256} inactive protein (right). (A) Protein gel of the soluble fraction (L), flow though (FT) and eluted fractions across the peak that were collected after Ni^{2+} affinity chromatography. 10 μL of the protein samples were separated by SDS-PAGE and visualised by InstantBlue Protein Stain. (B) Protein gel of the sample before overnight dialysis with protease 3C for the removal of the his-tag (T), after overnight dialysis (U) and flow through and eluted fractions across the peaks collected after the second Ni^{2+} affinity chromatography. (C) Protein gel of the diluted (Di) and concentrated (Co) samples before application to a HiLoad 16/600 S75pg column and eluted fractions collected after size-exclusion chromatography.
(TIF)

S1 Table. *Leishmania mexicana* C12, C19 and C65 deubiquitinases.
(DOCX)

S2 Table. Proteins specifically affinity-enriched with Cy5UbPRG.
(DOCX)

S3 Table. Oligonucleotide primers.
(DOCX)

S4 Table. Bar-seq data.
(XLSX)

S5 Table. DUB2 interacting partner data.
(XLSX)

S6 Table. DUB2 ubiquitination and phosphorylation sites.
(XLSX)

Acknowledgments

Author Contributions

Conceptualization: Andreas Damianou, Rebecca J. Burge, Carolina M. C. Catta-Preta, Vincent Geoghegan, Boris Rodenko, Jeremy C. Mottram.

Data curation: Vincent Geoghegan, Katherine Newling.

Funding acquisition: Boris Rodenko, Jeremy C. Mottram.

Investigation: Andreas Damianou, Rebecca J. Burge, Carolina M. C. Catta-Preta, Vincent Geoghegan, Y. Romina Nievas, Katherine Newling, Elaine Brown.

Resources: Vincent Geoghegan, Katherine Newling.

Supervision: Richard Burchmore, Boris Rodenko, Jeremy C. Mottram.

Visualization: Andreas Damianou, Rebecca J. Burge.

Writing – original draft: Andreas Damianou, Rebecca J. Burge, Vincent Geoghegan, Jeremy C. Mottram.

Writing – review & editing: Andreas Damianou, Rebecca J. Burge, Carolina M. C. Catta-Preta, Vincent Geoghegan, Y. Romina Nievas, Richard Burchmore, Boris Rodenko, Jeremy C. Mottram.

References

1. Barrett MP, Croft SL. Management of trypanosomiasis and leishmaniasis. Br Med Bull. 2012; 104:175–96. https://doi.org/10.1093/bmb/lds031 PMID: 23137768

2. Gluenz E, Wheeler RJ, Hughes L, Vaughan S. Scanning and three-dimensional electron microscopy methods for the study of *Trypanosoma brucei* and *Leishmania mexicana* flagella. Methods Cell Biol. 2015; 127:509–42. https://doi.org/10.1016/bs.mcb.2014.12.011 PMID: 25837406

3. Tsigankov P, Gherardini PF, Helmer-Citterich M, Spath GF, Myler PJ, Zilberstein D. Regulation dynamics of *Leishmania* differentiation: deconvoluting signals and identifying phosphorylation trends. Mol Cell Proteomics. 2014; 13(7):1787–99. https://doi.org/10.1074/mcp.M114.037705 PMID: 24741111

4. Cayla M, Rachidi N, Leclercq O, Schmidt-Arras D, Rosenqvist H, Wiese M, et al. Transgenic analysis of the *Leishmania* MAP kinase MPK10 reveals an auto-inhibitory mechanism crucial for stage-regulated activity and parasite viability. PLoS Pathog. 2014; 10(9):e1004347. https://doi.org/10.1371/journal.ppat.1004347 PMID: 25232945

5. Morales MA, Watanabe R, Dacher M, Chafey P, Osorio y Fortea J, Scott DA, et al. Phosphoproteome dynamics reveal heat-shock protein complexes specific to the *Leishmania donovani* infectious stage. Proc Natl Acad Sci U S A. 2010; 107(18):8381–6. https://doi.org/10.1073/pnas.0914768107 PMID: 20404152

6. Williams RA, Smith TK, Cull B, Mottram JC, Coombs GH. ATG5 is essential for ATG8-dependent autophagy and mitochondrial homeostasis in *Leishmania major*. PLoS Pathog. 2012; 8(5):e1002695. https://doi.org/10.1371/journal.ppat.1002695 PMID: 22615560

7. Cull B, Prado Godinho JL, Fernandes Rodrigues JC, Frank B, Schurigt U, Williams RA, et al. Glycosome turnover in *Leishmania* major is mediated by autophagy. Autophagy. 2014; 10(12):2143–57. https://doi.org/10.4161/auto.36438 PMID: 25484087

8. Casgrain PA, Martel C, McMaster WR, Mottram JC, Olivier M, Descoteaux A. Cysteine Peptidase B Regulates *Leishmania mexicana* Virulence through the Modulation of GP63 Expression. PLoS Pathog. 2016; 12(5):e1005658. https://doi.org/10.1371/journal.ppat.1005658 PMID: 27191844

9. Khare S, Nagle AS, Biggart A, Lai YH, Liang F, Davis LC, et al. Proteasome inhibition for treatment of leishmaniasis, Chagas disease and sleeping sickness. Nature. 2016; 537(7619):229–33. https://doi.org/10.1038/nature19339 PMID: 27501246

10. Wyllie S, Brand S, Thomas M, De Rycker M, Chung CW, Pena I, et al. Preclinical candidate for the treatment of visceral leishmaniasis that acts through proteasome inhibition. Proc Natl Acad Sci U S A. 2019; 116(19):9318–23. https://doi.org/10.1073/pnas.1820175116 PMID: 30962368

11. Ravid T, Hochstrasser M. Diversity of degradation signals in the ubiquitin-proteasome system. Nat Rev Mol Cell Biol. 2008; 9(9):679–90. https://doi.org/10.1038/nrm2468 PMID: 18698327

12. Wilkinson KD. Regulation of ubiquitin-dependent processes by deubiquitinating enzymes. FASEB J. 1997; 11(14):1245–56. https://doi.org/10.1096/fasebj.11.14.9409543 PMID: 9409543

13. Mevissen TET, Komander D. Mechanisms of Deubiquitinase Specificity and Regulation. Annu Rev Biochem. 2017; 86:159–92. https://doi.org/10.1146/annurev-biochem-061516-044916 PMID: 28498721

14. Rawlings ND, Barrett AJ, Thomas PD, Huang X, Bateman A, Finn RD. The MEROPS database of proteolytic enzymes, their substrates and inhibitors in 2017 and a comparison with peptidases in the PANTHER database. Nucleic Acids Res. 2018; 46(D1):D624–D32. https://doi.org/10.1093/nar/gkx1134 PMID: 29145643

15. Hermanns T, Pichlo C, Woiwode I, Klopffleisch K, Witting KF, Ovaa H, et al. A family of unconventional deubiquitinases with modular chain specificity determinants. Nat Commun. 2018; 9(1):799. https://doi.org/10.1038/s41467-018-03148-5 PMID: 29476094

16. Finn RD, Attwood TK, Babbitt PC, Bateman A, Bork P, Bridge AJ, et al. InterPro in 2017-beyond protein family and domain annotations. Nucleic Acids Res. 2017; 45(D1):D190–D9. https://doi.org/10.1093/nar/gkw1107 PMID: 27899635

17. Hofmann K, Bucher P. The UBA domain: a sequence motif present in multiple enzyme classes of the ubiquitination pathway. Trends Biochem Sci. 1996; 21(5):172–3. PMID: 8871400

18. Bonnet J, Romier C, Tora L, Devys D. Zinc-finger UBPs: regulators of deubiquitylation. Trends Biochem Sci. 2008; 33(8):369–75. https://doi.org/10.1016/j.tibs.2008.05.005 PMID: 18603431

19. Yamashita A, Chang TC, Yamashita Y, Zhu W, Zhong Z, Chen CY, et al. Concerted action of poly(A) nucleases and decapping enzyme in mammalian mRNA turnover. Nat Struct Mol Biol. 2005; 12 (12):1054–63. https://doi.org/10.1038/nsmb1016 PMID: 16284618

20. Quesada V, Diaz-Perales A, Gutierrez-Fernandez A, Garabaya C, Cal S, Lopez-Otin C. Cloning and enzymatic analysis of 22 novel human ubiquitin-specific proteases. Biochem Biophys Res Commun. 2004; 314(1):54–62. https://doi.org/10.1016/j.bbrc.2003.12.050 PMID: 14715245

21. Yang S, Liu L, Cao C, Song N, Wang Y, Ma S, et al. USP52 acts as a deubiquitinase and promotes histone chaperone ASF1A stabilization. Nat Commun. 2018; 9(1):1285. https://doi.org/10.1038/s41467-018-03588-z PMID: 29599486

22. Ekkebus R, van Kasteren SI, Kulathu Y, Scholten A, Berlin I, Geurink PP, et al. On terminal alkynes that can react with active-site cysteine nucleophiles in proteases. J Am Chem Soc. 2013; 135(8):2867–70. https://doi.org/10.1021/ja309802n PMID: 23387960

23. Beneke T, Madden R, Makin L, Valli J, Sunter J, Gluenz E. A CRISPR Cas9 high-throughput genome editing toolkit for kinetoplastids. R Soc Open Sci. 2017; 4(5):170095. https://doi.org/10.1098/rsos.170095 PMID: 28573017

24. Pinto-Fernandez A, Davis S, Schofield AB, Scott HC, Zhang P, Salah E, et al. Comprehensive Landscape of Active Deubiquitinating Enzymes Profiled by Advanced Chemoproteomics. Front Chem. 2019; 7:592. https://doi.org/10.3389/fchem.2019.00592 PMID: 31555637

25. Smith AM, Heisler LE, Mellor J, Kaper F, Thompson MJ, Chee M, et al. Quantitative phenotyping via deep barcode sequencing. Genome Res. 2009; 19(10):1836–42. https://doi.org/10.1101/gr.093955.109 PMID: 19622793

26. Grewal JS, Catta-Preta CMC, Brown E, Anand J, Mottram JC. Evaluation of clan CD C11 peptidase PNT1 and other *Leishmania mexicana* cysteine peptidases as potential drug targets. Biochimie. 2019; 166:150–60. https://doi.org/10.1016/j.biochi.2019.08.015 PMID: 31472179

27. Doehl JS, Sadlova J, Aslan H, Pruzinova K, Metangmo S, Votypka J, et al. *Leishmania* HASP and SHERP Genes Are Required for In Vivo Differentiation, Parasite Transmission and Virulence Attenuation in the Host. PLoS Pathog. 2017; 13(1):e1006130. https://doi.org/10.1371/journal.ppat.1006130 PMID: 28095465

28. Isogai S, Morimoto D, Arita K, Unzai S, Tenno T, Hasegawa J, et al. Crystal structure of the ubiquitin-associated (UBA) domain of p62 and its interaction with ubiquitin. J Biol Chem. 2011; 286(36):31864–74. https://doi.org/10.1074/jbc.M111.259630 PMID: 21715324

29. Duncan SM, Myburgh E, Philipon C, Brown E, Meissner M, Brewer J, et al. Conditional gene deletion with DiCre demonstrates an essential role for CRK3 in *Leishmania mexicana* cell cycle regulation. Mol Microbiol. 2016; 100(6):931–44. https://doi.org/10.1111/mmi.13375 PMID: 26991545

30. Badjatia N, Park SH, Ambrosio DL, Kirkham JK, Gunzl A. Cyclin-Dependent Kinase CRK9, Required for Spliced Leader trans Splicing of Pre-mRNA in Trypanosomes, Functions in a Complex with a New L-Type Cyclin and a Kinetoplastid-Specific Protein. PLoS Pathog. 2016; 12(3):e1005498. https://doi.org/10.1371/journal.ppat.1005498 PMID: 26954683

31. Andrews AJ, Chen X, Zevin A, Stargell LA, Luger K. The histone chaperone Nap1 promotes nucleosome assembly by eliminating nonnucleosomal histone DNA interactions. Mol Cell. 2010; 37(6):834–42. https://doi.org/10.1016/j.molcel.2010.01.037 PMID: 20347425

32. Bienko M, Green CM, Crosetto N, Rudolf F, Zapart G, Coull B, et al. Ubiquitin-binding domains in Y-family polymerases regulate translesion synthesis. Science. 2005; 310(5755):1821–4. https://doi.org/10.1126/science.1120615 PMID: 16357261

33. Besteiro S, Williams RA, Morrison LS, Coombs GH, Mottram JC. Endosome sorting and autophagy are essential for differentiation and virulence of *Leishmania major*. J Biol Chem. 2006; 281(16):11384–96. https://doi.org/10.1074/jbc.M512307200 PMID: 16497676

34. Besteiro S, Williams RA, Coombs GH, Mottram JC. Protein turnover and differentiation in *Leishmania*. Int J Parasitol. 2007; 37(10):1063–75. https://doi.org/10.1016/j.ijpara.2007.03.008 PMID: 17493624

35. Finley D, Ulrich HD, Sommer T, Kaiser P. The ubiquitin-proteasome system of *Saccharomyces cerevisiae*. Genetics. 2012; 192(2):319–60. https://doi.org/10.1534/genetics.112.140467 PMID: 23028185

36. Saunders EC, Ng WW, Kloehn J, Chambers JM, Ng M, McConville MJ. Induction of a stringent metabolic response in intracellular stages of *Leishmania mexicana* leads to increased dependence on mitochondrial metabolism. PLoS Pathog. 2014; 10(1):e1003888. https://doi.org/10.1371/journal.ppat.1003888 PMID: 24465208

37. Leifso K, Cohen-Freue G, Dogra N, Murray A, McMaster WR. Genomic and proteomic expression analysis of *Leishmania* promastigote and amastigote life stages: the *Leishmania* genome is constitutively

expressed. Mol Biochem Parasitol. 2007; 152(1):35–46. https://doi.org/10.1016/j.molbiopara.2006.11.009 PMID: 17188763

38. Williams RA, Tetley L, Mottram JC, Coombs GH. Cysteine peptidases CPA and CPB are vital for autophagy and differentiation in *Leishmania mexicana*. Mol Microbiol. 2006; 61(3):655–74. https://doi.org/10.1111/j.1365-2958.2006.05274.x PMID: 16803590

39. Mottram JC, Brooks DR, Coombs GH. Roles of cysteine proteinases of trypanosomes and *Leishmania* in host-parasite interactions. Curr Opin Microbiol. 1998; 1(4):455–60. https://doi.org/10.1016/s1369-5274(98)80065-9 PMID: 10066510

40. Barak E, Amin-Spector S, Gerliak E, Goyard S, Holland N, Zilberstein D. Differentiation of *Leishmania donovani* in host-free system: analysis of signal perception and response. Mol Biochem Parasitol. 2005; 141(1):99–108. https://doi.org/10.1016/j.molbiopara.2005.02.004 PMID: 15811531

41. Grou CP, Pinto MP, Mendes AV, Domingues P, Azevedo JE. The de novo synthesis of ubiquitin: identification of deubiquitinases acting on ubiquitin precursors. Sci Rep. 2015; 5:12836. https://doi.org/10.1038/srep12836 PMID: 26235645

42. Sun XX, He X, Yin L, Komada M, Sears RC, Dai MS. The nucleolar ubiquitin-specific protease USP36 deubiquitinates and stabilizes c-Myc. Proc Natl Acad Sci U S A. 2015; 112(12):3734–9. https://doi.org/10.1073/pnas.1411713112 PMID: 25775507

43. Fraile JM, Campos-Iglesias D, Rodriguez F, Astudillo A, Vilarrasa-Blasi R, Verdaguer-Dot N, et al. Loss of the deubiquitinase USP36 destabilizes the RNA helicase DHX33 and causes preimplantation lethality in mice. J Biol Chem. 2018; 293(6):2183–94. https://doi.org/10.1074/jbc.M117.788430 PMID: 29273634

44. Richardson LA, Reed BJ, Charette JM, Freed EF, Fredrickson EK, Locke MN, et al. A conserved deubiquitinating enzyme controls cell growth by regulating RNA polymerase I stability. Cell Rep. 2012; 2 (2):372–85. https://doi.org/10.1016/j.celrep.2012.07.009 PMID: 22902402

45. Coornaert B, Baens M, Heyninck K, Bekaert T, Haegman M, Staal J, et al. T cell antigen receptor stimulation induces MALT1 paracaspase-mediated cleavage of the NF-kappaB inhibitor A20. Nat Immunol. 2008; 9(3):263–71. https://doi.org/10.1038/ni1561 PMID: 18223652

46. Staal J, Driege Y, Bekaert T, Demeyer A, Muyllaert D, Van Damme P, et al. T-cell receptor-induced JNK activation requires proteolytic inactivation of CYLD by MALT1. EMBO J. 2011; 30(9):1742–52. https://doi.org/10.1038/emboj.2011.85 PMID: 21448133

47. Reyes-Turcu FE, Shanks JR, Komander D, Wilkinson KD. Recognition of polyubiquitin isoforms by the multiple ubiquitin binding modules of isopeptidase T. J Biol Chem. 2008; 283(28):19581–92. https://doi.org/10.1074/jbc.M800947200 PMID: 18482987

48. Reyes-Turcu FE, Horton JR, Mullally JE, Heroux A, Cheng X, Wilkinson KD. The ubiquitin binding domain ZnF UBP recognizes the C-terminal diglycine motif of unanchored ubiquitin. Cell. 2006; 124 (6):1197–208. https://doi.org/10.1016/j.cell.2006.02.038 PMID: 16564012

49. Zhang YH, Zhou CJ, Zhou ZR, Song AX, Hu HY. Domain analysis reveals that a deubiquitinating enzyme USP13 performs non-activating catalysis for Lys63-linked polyubiquitin. PLoS One. 2011; 6 (12):e29362. https://doi.org/10.1371/journal.pone.0029362 PMID: 22216260

50. Clayton C. Regulation of gene expression in trypanosomatids: living with polycistronic transcription. Open Biol. 2019; 9(6):190072. https://doi.org/10.1098/rsob.190072 PMID: 31164043

51. Park Y, Jin HS, Liu YC. Regulation of T cell function by the ubiquitin-specific protease USP9X via modulating the Carma1-Bcl10-Malt1 complex. Proc Natl Acad Sci U S A. 2013; 110(23):9433–8. https://doi.org/10.1073/pnas.1221925110 PMID: 23690623

52. Fleming AB, Kao CF, Hillyer C, Pikaart M, Osley MA. H2B ubiquitylation plays a role in nucleosome dynamics during transcription elongation. Mol Cell. 2008; 31(1):57–66. https://doi.org/10.1016/j.molcel.2008.04.025 PMID: 18614047

53. Huang OW, Ma X, Yin J, Flinders J, Maurer T, Kayagaki N, et al. Phosphorylation-dependent activity of the deubiquitinase DUBA. Nat Struct Mol Biol. 2012; 19(2):171–5. https://doi.org/10.1038/nsmb.2206 PMID: 22245969

54. Meray RK, Lansbury PT Jr., Reversible monoubiquitination regulates the Parkinson disease-associated ubiquitin hydrolase UCH-L1. J Biol Chem. 2007; 282(14):10567–75. https://doi.org/10.1074/jbc.M611153200 PMID: 17259170

55. Akutsu M, Dikic I, Bremm A. Ubiquitin chain diversity at a glance. J Cell Sci. 2016; 129(5):875–80. https://doi.org/10.1242/jcs.183954 PMID: 26906419

56. Harrigan JA, Jacq X, Martin NM, Jackson SP. Deubiquitylating enzymes and drug discovery: emerging opportunities. Nat Rev Drug Discov. 2018; 17(1):57–78. https://doi.org/10.1038/nrd.2017.152 PMID: 28959952

57. Turnbull AP, Ioannidis S, Krajewski WW, Pinto-Fernandez A, Heride C, Martin ACL, et al. Molecular basis of USP7 inhibition by selective small-molecule inhibitors. Nature. 2017; 550(7677):481–6. https://doi.org/10.1038/nature24451 PMID: 29045389

58. Kategaya L, Di Lello P, Rouge L, Pastor R, Clark KR, Drummond J, et al. USP7 small-molecule inhibitors interfere with ubiquitin binding. Nature. 2017; 550(7677):534–8. https://doi.org/10.1038/nature24006 PMID: 29045385

59. Lee BH, Lee MJ, Park S, Oh DC, Elsasser S, Chen PC, et al. Enhancement of proteasome activity by a small-molecule inhibitor of USP14. Nature. 2010; 467(7312):179–84. https://doi.org/10.1038/nature09299 PMID: 20829789

60. Jones NG, Catta-Preta CMC, Lima A, Mottram JC. Genetically Validated Drug Targets in *Leishmania*: Current Knowledge and Future Prospects. ACS Infect Dis. 2018; 4(4):467–77. https://doi.org/10.1021/acsinfecdis.7b00244 PMID: 29384366

61. Bates PA, Robertson CD, Tetley L, Coombs GH. Axenic cultivation and characterization of *Leishmania mexicana* amastigote-like forms. Parasitology. 1992; 105 (Pt 2):193–202.

62. Sunter JD, Yanase R, Wang Z, Catta-Preta CMC, Moreira-Leite F, Myskova J, et al. *Leishmania* flagellum attachment zone is critical for flagellar pocket shape, development in the sand fly, and pathogenicity in the host. Proc Natl Acad Sci U S A. 2019; 116(13):6351–60. https://doi.org/10.1073/pnas.1812462116 PMID: 30850532

63. Hart DT, Vickerman K, Coombs GH. A quick, simple method for purifying *Leishmania mexicana* amastigotes in large numbers. Parasitology. 1981; 82(Pt 3):345–55. https://doi.org/10.1017/s0031182000066889 PMID: 7243344

64. The UniProt C. UniProt: the universal protein knowledgebase. Nucleic Acids Res. 2017; 45(D1):D158–D69. https://doi.org/10.1093/nar/gkw1099 PMID: 27899622

65. Kozlov AM, Darriba D, Flouri T, Morel B, Stamatakis A. RAxML-NG: a fast, scalable and user-friendly tool for maximum likelihood phylogenetic inference. Bioinformatics. 2019; 35(21):4453–5. https://doi.org/10.1093/bioinformatics/btz305 PMID: 31070718

66. Bringmann G, Thomale K, Bischof S, Schneider C, Schultheis M, Schwarz T, et al. A novel *Leishmania major* amastigote assay in 96-well format for rapid drug screening and its use for discovery and evaluation of a new class of leishmanicidal quinolinium salts. Antimicrob Agents Chemother. 2013; 57(7):3003–11. https://doi.org/10.1128/AAC.02201-12 PMID: 23587955

67. Teo G, Koh H, Fermin D, Lambert JP, Knight JD, Gingras AC, et al. SAINTq: Scoring protein-protein interactions in affinity purification—mass spectrometry experiments with fragment or peptide intensity data. Proteomics. 2016; 16(15–16):2238–45. https://doi.org/10.1002/pmic.201500499 PMID: 27119218